

10-2023

**DESIGN AND APPLICATION OF CIRCULAR EDGE-FED LINEARLY
POLARIZED PATCH ANTENNA WITH ENHANCED BANDWIDTH
AND GAIN FOR RESPIRATORY MONITORING SYSTEMS**

Mo'ath Akram AL Hayek

Follow this and additional works at: https://scholarworks.uaeu.ac.ae/all_theses

 Part of the [Engineering Commons](#)



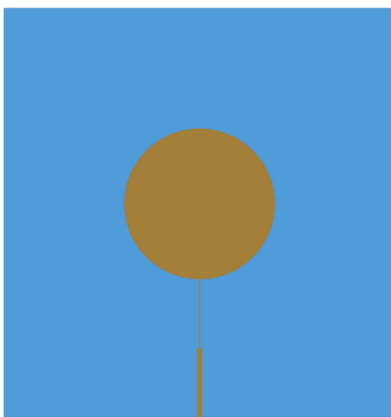
MASTER THESIS NO. 2023: 77

College of Engineering

Department of Electrical and Communication Engineering

**DESIGN AND APPLICATION OF CIRCULAR EDGE-FED
LINEARLY POLARIZED PATCH ANTENNA WITH ENHANCED
BANDWIDTH AND GAIN FOR RESPIRATORY MONITORING
SYSTEMS**

Mo'ath Akram AL Hayek



October 2023

United Arab Emirates University

College of Engineering

Department of Electrical and Communication Engineering

DESIGN AND APPLICATION OF CIRCULAR EDGE-FED
LINEARLY POLARIZED PATCH ANTENNA WITH ENHANCED
BANDWIDTH AND GAIN FOR RESPIRATORY MONITORING
SYSTEMS

Mo'ath Akram Al Hayek

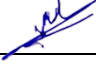
This thesis is submitted in partial fulfilment of the requirements for the degree of Master
of Science in Electrical Engineering

October 2023

Cover: Circular edge-fed linearly polarized patch antenna
(Photo: By Mo'ath Akram Al Hayek)

Declaration of Original Work

I, Mo'ath Akram Al Hayek, the undersigned, a graduate student at the United Arab Emirates University (UAEU), and the author of this thesis entitled "*Design and Application of Circular Edge-Fed Linearly Polarized Patch Antenna with Enhanced Bandwidth and Gain For Respiratory Monitoring Systems*", hereby, solemnly declare that this is the original research work done by me under the supervision of Prof. Mousa Hussein, in the College of Engineering at UAEU. This work has not previously formed the basis for the award of any academic degree, diploma or a similar title at this or any other university. Any materials borrowed from other sources (whether published or unpublished) and relied upon or included in my thesis have been properly cited and acknowledged in accordance with appropriate academic conventions. I further declare that there is no potential conflict of interest with respect to the research, data collection, authorship, presentation and/or publication of this thesis.

Student's Signature:  _____

Date: 10th Sep 2023

Advisory Committee

1) Advisor: Mousa Hussain

Title: Professor

Department of Electrical and Communication Engineering

College of Engineering

2) Co-advisor: Mohamed Abdelaal

Title: Associate Professor

Department of Electrical and Communication Engineering

College of Engineering

Approval of the Master Thesis

This Master Thesis is approved by the following Examining Committee Members:

- 1) Advisor (Committee Chair): Mousa Hussein

Title: Professor

Department of Electrical and Communication Engineering

College of Engineering

Signature 


Date Nov 22nd, 2023

- 2) Member: Mohamed AL Khatib

Title: Assistant Professor

Department of Electrical and Communication Engineering

College of Engineering

Signature 

Date Nov 22nd, 2023

- 3) Member (External Examiner): Tayeb A. Denidni

Title: Full Professor

Department of Radio Frequency Laboratory

Institution: Institut national de la recherche scientifique, Canada

Signed by Prof. Falah Awwad 

Date Nov. 22, 2023

This Master Thesis is accepted by:

Dean of the College of Engineering: Professor Mohamed H. Al Marzouqi

Signature Mohamed AlMarzouqi

Date November 28, 2023

Dean of the College of Graduate Studies: Professor Ali Al-Marzouqi

Signature Ali Hassan

Date 28/11/2023

Abstract

This Master's thesis explores the design and application of a circular edge-fed patch antenna for respiratory monitoring systems. The antenna, fabricated from a thin copper adhesive sheet, demonstrates compatibility with textile materials of low thickness and a relative permittivity of 1.3. Using CST Studio Suite 3D EM simulation software, the antenna's design was optimized through extensive trials, achieving improved bandwidth and gain. Our findings indicate that the antenna successfully differentiates between various breathing patterns, including slow, normal, and fast breathing rates. The study's managerial and research implications extend to healthcare, wearable technology sectors, and the broader scientific community. The research not only presents novel insights within the field of antenna design for respiratory monitoring but also establishes a robust foundation for future exploration in this domain.

Keywords: Circular Edge-fed Patch Antenna, Respiratory Monitoring Systems, CST Studio Suite 3D EM simulation, Bandwidth, Gain, Breathing Patterns, Healthcare, Wearable Technology.

Title and Abstract (in Arabic)

تصميم وتطبيق الهوائي الدائري ذو التغذية الحافية المستقطبة خطيًا والمعزز بالنطاق الترددي والكسب لأنظمة مراقبة التنفس

الملخص

تستكشف هذه الأطروحة تصميم وتطبيق آلية دائرية تغذى على الحافة لأنظمة مراقبة التنفس. صُنعت الهوائي من ورقة نحاسية لاصقة رقيقة، وأظهرت التوافق مع مواد نسيجية ذات سمك منخفض وثابتة نسبية قدرها 1.3. باستخدام برنامج محاكاة ثلاثية الأبعاد لـ CST Studio Suite، تم تحسين تصميم الهوائي من خلال تجارب مكثفة، مما أسفر عن تحسين نطاق الترددات والكسب. تشير نتائجنا إلى أن الهوائي يفرق بنجاح بين أنماط التنفس المختلفة، بما في ذلك معدلات التنفس البطيئة والطبيعية والسريعة. تمتد آثار الدراسة الإدارية والبحثية إلى الرعاية الصحية، وقطاعات التكنولوجيا القابلة للارتداء، والمجتمع العلمي الأوسع. البحث لا يقدم فقط رؤى جديدة في مجال تصميم الهوائي لمراقبة التنفس ولكنه أيضًا ينشئ أساسًا قويًا للتنقيب المستقبلي في هذا المجال.

مفاهيم البحث الرئيسية: هوائي دائري تغذى على الحافة، أنظمة مراقبة التنفس، محاكاة ثلاثية الأبعاد لـ CST Studio Suite، نطاق الترددات الكسب، أنماط التنفس، الرعاية الصحية، التكنولوجيا القابلة للارتداء.

Author Profile

Mo'ath Akram AL Hayek is an electrical power engineer with over four years of experience in research and education. He is currently working at Abu Dhabi Vocational and Training Institution (ADVETI) and resides in the UAE with his family. Mo'ath received his bachelor's degree from AL Balqa Applied University in Jordan, graduating with top honors in the top 3% of his class.

During his time at AL Balqa Applied University, Mo'ath was a co-founder and chairperson of the IEEE student branch. He and his team were recognized with several national and international awards for their outstanding work and contributions to the field, including the successful organization of international conferences. Mo'ath has also received over four international recognitions from IEEE for his contributions to the field. Mo'ath is a dedicated individual who is committed to making a positive impact in his field. His passion for excellence and leadership has made him an invaluable asset to the engineering community.

Acknowledgements

I would like to express my sincere gratitude to my thesis advisor, Prof. Mousa, for his invaluable guidance, support, and encouragement throughout the research. His expertise and insights have been crucial to the successful completion of this work.

Furthermore, I would like to thank Dr. Adamu for his continuous support and guidance during this research. His expertise in the field has been an invaluable resource, and his encouragement has been a constant source of motivation for me.

Dedication

To my father, mother, wife Raghad, and daughter Zaina. You have been my pillars of strength, my source of inspiration, and my reason to strive for excellence. Your unwavering support and love have made this journey possible, and I dedicate this achievement to you.

Table of Contents

Title.....	i
Declaration of Original Work.....	iii
Advisory Committee.....	iv
Approval of the Master Thesis.....	v
Abstract.....	vii
Title and Abstract (in Arabic).....	viii
Author Profile	ix
Acknowledgements.....	x
Dedication	xi
Table of Contents.....	xii
List of Tables	xiv
List of Figures.....	xv
List of Abbreviations	xvii
Chapter 1: Introduction.....	1
1.1 Overview	2
1.2 Statement of the Problem	2
1.3 Research Objectives	3
1.4 Relevant Literature	4
1.4.1 Microstrip Patch Antenna	5
1.4.2 Breathing Mechanism	6
1.4.3 Potential Contributions and Limitations of the Study.....	7
Chapter 2: Circular Edge-Fed Microstrip Patch Antenna Design	10
2.1 Research Design.....	10
2.2 Design Using CST studio	15
Chapter 3: Results and Discussions	18
3.1 Design and Characteristics of the Microstrip Patch Antenna.....	18
3.2 Practical Microstrip Patch Antenna and Equipment Used	23
3.3 Results of Different Breathing Patterns.....	26
3.4 Breathing Rate Estimation.....	35
Chapter 4: Conclusion	44
4.1 Managerial Implications.....	44

4.2 Research Implications	44
4.3 Research Limitations	45
4.4 Future Work and Improvements.....	45
References.....	46
Appendix.....	50

List of Tables

Table 1: Comparison of the proposed breathing sensor with related work	9
Table 2: Proposed Antenna Parameters	15
Table 3: S11 values under normal breathing pattern	31
Table 4: S11 values under slow breathing pattern.....	32
Table 5: S11 values under fast breathing pattern.....	33
Table 6: Summary of different breathing pattern in terms of frequency, S11, Phase and Breathing rate	42

List of Figures

Figure 1.1: The basic structure of the microstrip patch antenna.....	5
Figure 1.2: Four common feeding methods of microstrip patch antenna.....	6
Figure 1.3: Air volume change in the lungs during breathing	7
Figure 2.1: Basic drawing of a circular edge-fed patch antenna indicating the parameters	11
Figure 2.2: Circular edge-fed patch antenna using CST Studio software.	16
Figure 2.3: Circular edge-fed patch antenna final product.....	16
Figure 3.1: Circular edge-fed patch antenna design using CST	18
Figure 3.2: Simulated return loss (S11) for the circular patch antenna	20
Figure 3.3: Simulated return loss (S11) for calculating the bandwidth of the circular patch antenna.	21
Figure 3.4: Simulated VSWR of the circular patch antenna.....	21
Figure 3.5: Simulated realized gain of the circular patch antenna.....	22
Figure 3.6: Simulated radiation efficiency of the circular patch antenna.	22
Figure 3.7: Simulated Far field of the circular patch antenna.....	23
Figure 3.8: Circular patch antenna with stretchable textile substrate	24
Figure 3.9: Circular patch antenna with stretchable textile substrate soldered to SMA connector.....	24
Figure 3.10: Circular patch antenna placed on the stretchable textile substrate along with the ground plane.	25
Figure 3.11: Rohde and Schwarz ZVL13 Vector Network Analyzer (VNA)	26
Figure 3.12: Rohde and Schwarz ZVL13 (VNA) calibration parts	26
Figure 3.13: Return loss curve for simulated and practical antenna.....	28
Figure 3.14: Return loss curve for multiple trials	29
Figure 3.15: Return loss curve for multiple trials under normal breathing pattern	30
Figure 3.16: Return loss phase curve for multiple trials under normal breathing pattern.....	31
Figure 3.17: Return loss curve for multiple trials under slow breathing pattern	32
Figure 3.18: Return loss phase curve for multiple trials under slow breathing pattern ...	33
Figure 3.19: Return loss curve for multiple trials under fast breathing pattern.....	34
Figure 3.20: Return loss phase curve for multiple trials under fast breathing pattern....	34
Figure 3.21: Return loss curves comparison between different breathing patterns and no breathing.....	35
Figure 3.22: Flowchart of the Breathing Rate Estimation Process.....	38
Figure 3.23: Magnitude of IFFT of S11 under normal breathing.....	39
Figure 3.24: Magnitude of dBm of IFFT of S11 under normal breathing.....	40
Figure 3.25: Magnitude of IFFT of S11 under fast breathing	40
Figure 3.26: Magnitude of dBm of IFFT of S11 under fast breathing	41
Figure 3.27: Magnitude of IFFT of S11 under slow breathing.....	41

Figure 3.28: Magnitude of dBm of IFFT of S11 under fast breathing 42

List of Abbreviations

BW	Bandwidth
CST	Computer Simulation Technology
dB	Decibels
EM	Electromagnetic
GHz	Giga Hertz
Mm	Millimeter
NCS	Near-field Coherent Sensing
PCB	Printed Circuit Board
RF	Radio Frequency
S11	Reflection Coefficient
SMA	Subminiature Version A
SOL	Short – Open – Load
VNA	Vector Network Analyzer
VSWR	Voltage Standing Wave Ratio

Chapter 1: Introduction

Antenna sensors have caught the attention of the research community in recent years because to their numerous advantages, including passive operation, cheap cost, easy design, and dual functionality of communication and sensing. The concept of using antenna sensors dates to the 1960s, when it was initially proposed by researchers. They discovered that physical changes to the antenna structure caused by interaction with the environment might induce a shift in its resonance frequency, which could be utilized to detect a variety of physical factors [1]. In recent years, researchers have been exploring the exciting potential of using antenna sensors in a range of different fields, from monitoring the environment to tracking the health of agricultural crops and even monitoring food production. One of the earliest uses of antenna sensors was in soil moisture monitoring, where circular antenna sensors were used to evaluate the relative permittivity of soil samples. This groundbreaking technology has paved the way for a wide range of innovative new applications, many of which have already been developed and implemented in real-world scenarios [2]. In the early 2000s, scientists started exploring the use of antenna sensors for structural health monitoring. They came up with an innovative method that involved a patch antenna acting as a strain sensor. This technology could effectively detect the shift in resonance frequency caused by deformation or vibration in the structure, thus measuring the strain. This technique could be utilized for monitoring the structural health of critical civil infrastructures such as bridges, buildings, and dams [3]. A group of researchers proposed a microstrip patch antenna for detecting human respiratory motions in 2007, ushering in a new use for antenna sensors in the medical industry [4]. This antenna was used to track patients' breathing patterns since it could detect movement of the chest wall during respiration. Since then, antenna sensors have been employed in a variety of additional medical applications, including glucose sensing, cancer diagnostics, and vital sign monitoring [5]. Because of their non-invasive nature and ease of use, antenna sensors have shown to be a promising technology for medical applications [6]. Antenna sensors have increased in prominence in the world of wearable electronics because to their exciting potential for health monitoring and fitness tracking. Antenna sensors included in wearable devices such as smartwatches, fitness bands, and e-textiles provide non-invasive continuous monitoring of vital parameters such

as heart rate, respiration rate, and body temperature. The accuracy and dependability of these sensors in monitoring vital signs have been demonstrated in research studies, opening the way for their widespread use in healthcare applications. Moreover, antenna sensors integrated into wearable devices offer a number of advantages such as mobility, simplicity, and ease of use, making them an interesting option for health monitoring [7]. Because of its low production cost, compact size, durability and dependability, and lightweight, microstrip patch antennas have been widely employed in sensing applications. The interplay of electromagnetic waves and dielectric characteristics underpins the operation of patch antennas as sensors. In fact, earlier research has created a sensor that uses a microstrip patch antenna on a flame retardant 4 (FR-4) substrate [8].

1.1 Overview

Wearable devices for health monitoring applications have attracted substantial interest in recent years because of their potential for continuous and non-invasive monitoring of vital indicators such as heart rate, respiration rate, and body temperature. The antenna sensor, which enables wireless connection and data transfer, is a critical component of these wearable devices. We present a new circular slotted broadband patch antenna with increased gain and bandwidth for high-accuracy health monitoring applications. The antenna is intended to be incorporated into wearable devices such as smartwatches, fitness bands as well as casual clothing to provide accurate real-time monitoring of vital indicators. The proposed antenna design offers better performance for applications involving health monitoring while addressing the drawbacks of earlier antenna designs, such as their limited bandwidth and low gain. The goal of the project is to enhance and improve wearable technology for applications such as health monitoring.

1.2 Statement of the Problem

The escalating healthcare expenditures have become a big worry for many nations, as healthcare bills represent a large component of the national budget [9]. One of the main difficulties in healthcare is developing innovative methods for incorporating sensors into materials, such as clothes and bedding, to monitor persons' health state in real-time while providing optimal comfort [10]. Breathing is a crucial indicator that must be examined continually throughout medical treatment since it might suggest pathological instability

such as sleep apnea, asthma, lung illness, and cardiopulmonary arrest [11]. Constant monitoring of breathing is required to assess the subject's health state, and wearable technologies are seen as an important diagnostic tool in advancing healthcare outside of the hospital [12]. A sensor might be used as an alternative diagnostic instrument to detect vital physiological signals in humans in real time. However, there are considerable differences across methodologies, such as sensors and breathing parameters, sensing techniques, sensor location, sensor data processing, analytic software, and performance evaluation [13]. In this thesis, a new approach for breathing monitoring is proposed, which involves integrating a fully microstrip patch antenna sensor into a commercially available T-shirt. The sensor is designed to detect chest wall movements and provide accurate measurements of breathing patterns in real-time. The validation of this approach is also discussed.

1.3 Research Objectives

Antenna sensor networks have numerous potential applications in healthcare, including pervasive monitoring for distributed healthcare. While current commercial wearables can measure various vital signs in real-time, breathing sensors remain a challenging area of research. This thesis investigates the use of wearable antennas for respiration monitoring based on a low-profile fully textile antenna [26, 29]. The proposed antenna has a simple structure, does not require active mechanical sensing elements or specific materials, and exhibits over 10 dB wireless gain sensitivity to normal breathing. A peak-detection algorithm is used to show a high breath detection accuracy. Based on the experimental results, it is concluded that antennas can be utilized as highly accurate sensors for respiration monitoring without the need for specific sensing elements or materials. To develop such sensing antenna for vital sign monitoring, the antenna needs to remain in proximity to the human body for efficient operation. This is evaluated through the antenna's radiation efficiency and reflection coefficient, where a sufficiently low reflection (under 10%) indicates that the antenna can be integrated with different transmitters [26, 29]. Additionally, the antenna needs to be un-isolated from the human body to detect changes in dielectric properties induced by breathing through its gain. The sensing antenna is based on an edge-fed circular patch design, which is renowned for its compatibility with circuit board technology, its moderate gain, and efficiency on the body.

This patch antenna is distinct due to its smaller beam width, narrower bandwidth, and reduced physical area compared to its rectangular counterparts. Manufactured by placing the antenna patch element and feed network on a textile substrate, the design maintains a low-profile, ensuring its suitability for wearable applications without mandating a specific substrate thickness for optimal radiation. The antenna's design is bolstered by a sole substrate, contributing to its mechanical stability and electrical performance. The intrinsic flexibility of this design enables it to adapt to various body contours and movements, a critical attribute for wearable sensors aiming for user comfort and discretion. The operational mechanism sees the patch as a resonant cavity with a cylindrical radiating slot, extending from the patch perimeter to the ground plane. Summarily, the proposed sensing antenna for respiration monitoring stands out for its precision and streamlined design, positioning it as a prime choice for incorporation into wearable clothes tailored for distributed healthcare applications.

1.4 Relevant Literature

Researchers have found that body worn systems with sensing, processing, actuation, communication, and energy harvesting and storage abilities are a promising solution for monitoring people in various applications such as healthcare, lifestyle, protection, and safety [14]. The new generation of clothing is expected to have the ability to sense, communicate data, and harvest energy in a non-intrusive way [15]. To achieve optimal results, wearable antennas must be thin, lightweight, low maintenance, robust, inexpensive, and easily integrated into radio frequency (RF) circuits [16, 17]. Planar antennas are preferred because they allow excellent integration with RF circuits, feeding lines, and matching circuits on a standard multilayer board material, despite having lower maximum bandwidth-efficiency than the theoretical limit for electrically small antennas [16]. As a result, planar antennas can be integrated into clothing in a minimally intrusive way [18]. Microstrip patch antennas are particularly suitable for body-worn applications because they mainly radiate perpendicularly to the planar structure and efficiently shield the body tissues with their ground plane [18, 19]. Specific requirements for wearable antenna design include a planar structure, flexible conductive materials in the patch and ground plane, and flexible dielectric materials [20]. The characteristics of materials, such as the permittivity and thickness of the dielectric substrate, primarily determine the

bandwidth and efficiency performance of the planar antenna, while the conductivity of the ground plane and patch significantly affect the antenna's efficiency and should be as high as possible [21].

1.4.1 Microstrip Patch Antenna

Microstrip patch antennas arose from the use of printed circuit technology for not just circuit components and transmission lines, but also the radiating parts of an electronic system. Figure 1.1 depicts the fundamental construction of a microstrip patch antenna. It consists of a metallization region supported by a thin dielectric substrate over a ground plane and supplied against the ground at an appropriate place. Although any patch form can be utilized, the rectangle, circle, Equilateral triangle, and annular ring are the most common.

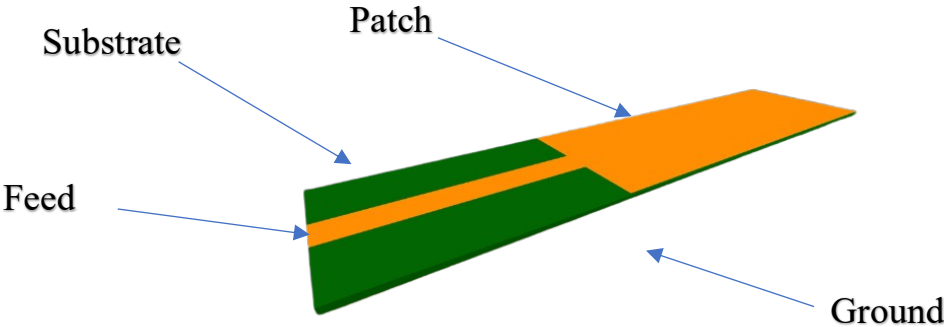


Figure 1.1: The basic structure of the microstrip patch antenna.

Four feeding methods are given in Figure 1.2: coaxial probe feed, microstrip line feed, aperture-coupled feed, and proximity feed.

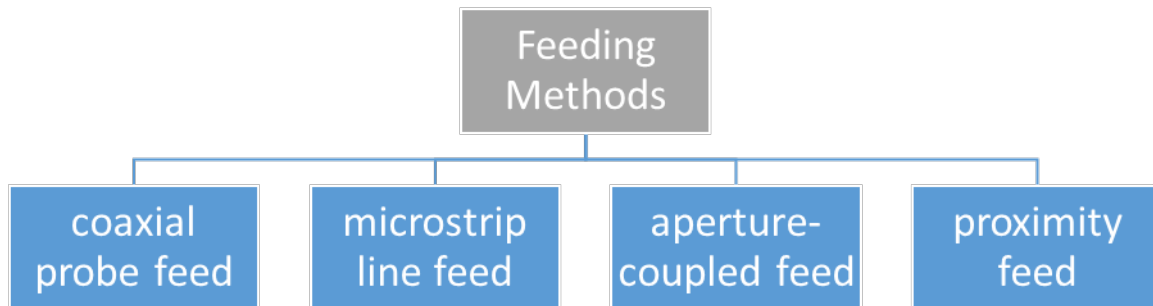


Figure 1.2: Four common feeding methods of microstrip patch antenna.

Electromagnetic radiation is directed or linked to the region underneath the patch, which acts as a resonant cavity with open circuits on both sides. Part of the energy escapes from the cavity and radiates into space, forming an antenna [22]. In electrical systems, microstrip patch antennas offer several benefits. They may be altered from their initial flat state to follow the contours of the surface they are put on. They are less intrusive as well due to their reduced radar cross-section and low radar profile. Printed circuit technology may be used to create durable microstrip patch antennas. They may also be easily combined with other circuit elements to create dual polarization and dual or multi-frequency operation.

1.4.2 Breathing Mechanism

Figure 1.3 shows a simplified illustration of the air volume change in the lungs during breathing. According to research, respiration causes a mechanical deformation and modification of dielectric properties in the human chest and abdomen due to the exchange of air between the lungs and the external environment.

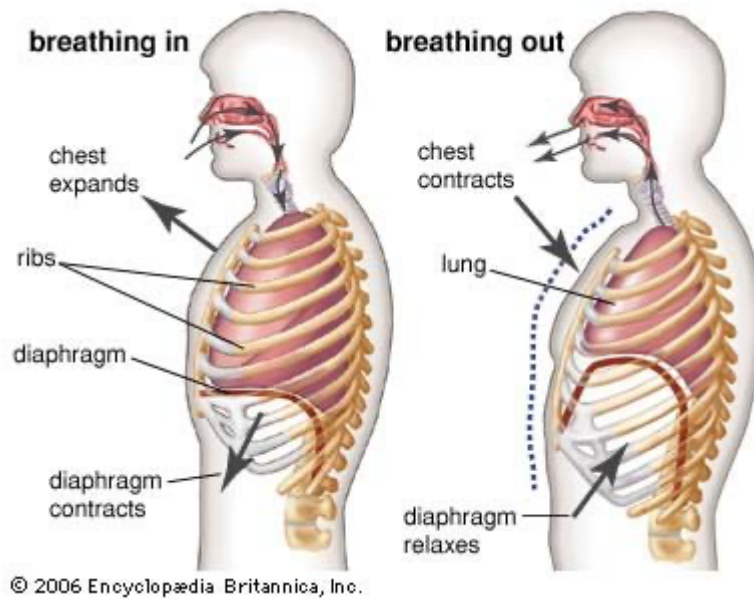


Figure 1.3: Air volume change in the lungs during breathing [41].

The contraction of the diaphragm during inhalation leads to the enlargement of the thoracic cavity and a decrease in intra-thoracic pressure, resulting in lung expansion. During exhalation, the diaphragm and inter-costal muscles relax, and the chest and abdomen return to the rest position. The tidal volume of normal breathing is estimated to be around 7 mL per kg of body mass, which is equivalent to the expansion of the chest circumference by 7.37 cm in 25–34-year-old males [23, 24]. The dielectric properties of the torso change noticeably during inhalation or exhalation, with the relative permittivity ϵ_r of inflated lungs at 2.45 GHz being $\epsilon_r = 20.51$ and that of deflated lungs being $\epsilon_r = 48.45$, according to [24]. While a highly sensitive sensor capable of detecting the physical deformation and change in dielectric properties of the medium is needed to detect breathing, this approach holds promise for detecting breathing-related anomalies in medical applications [23, 24].

1.4.3 Potential Contributions and Limitations of the Study

Based on the information from Table 1 we can conclude that the results presented in [26, 29] have some specific limitations that need to be addressed. First, the antenna's fabrication relies on conductive fabric, and while effective in their experiments, questions remain about the long-term durability and wear-and-tear of this material, especially under regular movement and varying environmental conditions. This limitation could impact the

practical applicability of the technology in long-term health monitoring scenarios. Second, the performance of the sensor appears to be significantly influenced by the sensitivity of the wireless receiver. This suggests that the maximum read range and, therefore, the generalizability of their findings, might be restricted by the specifications of different wireless communication systems or devices. Understanding these limitations could provide valuable directions for future research efforts in enhancing the durability of conductive fabrics and in exploring the antenna's compatibility with wireless receivers of varying sensitivities. On the other hand, Despite the promising results of [28] study on wearable antennas for healthcare monitoring, there are some limitations that need to be addressed. One limitation is the short range of the wireless communication platform, which may limit the applicability of the technology in certain scenarios. Another limitation is the sensitivity of the multimaterial fiber antenna with spiral geometry to physical deformation, which may affect the accuracy of the breath detection. Additionally, while the study demonstrated the capability of the sensor to detect breathing patterns in real-time and communicate the data via Bluetooth, further validation is needed to compare the performance of the sensor with gold standard equipment such as a spirometer or a pneumotachograph for medical applications. Finally, while the water-repelling properties of the coating applied to the fibers and textiles enhanced the environmental endurance of the smart textile, the long-term durability of the coating and its potential impact on the antenna performance need to be further investigated. Whereas One limitation of [25] proposed method for monitoring vital signs using near-field coherent sensing (NCS) is that it has not been validated for clinical use. The article states that the system could lead to cost-effective automation of vital sign monitoring in care facilities, but it is unclear if the system has been tested in a clinical setting. Furthermore, the article does not provide any information on the accuracy of the system compared to traditional methods for monitoring vital signs, such as direct skin contact sensors or invasive monitoring devices. Additional studies would be needed to evaluate the clinical usefulness and accuracy of the proposed method before it can be implemented in medical settings. Finally, [27] proposed wearable antenna, Belly patch, shows good on-body radiation efficiency and sensitivity to compression for monitoring respiration. However, the Belly patch is larger in size compared to other sensors, which may limit its application in certain situations.

Additionally, while the use of low-conductivity materials to improve bandwidth is promising, it may lead to reduced antenna gain, which may impact the maximum read range achievable. Therefore, further optimization of the antenna design is required to achieve a balance between size, bandwidth, gain, and read range.

Table 1: Comparison of the proposed breathing sensor with related work

	This work	[26]	[25]	[29]	[27]	[28]
Antenna material	Copper	Textile	PCB	Textile	Textile + Foam	Spiral fiber
Sensing mechanism	Vector Network Analyzer	Dielectric sensing	Dielectric sensing	Strain sensing	Compression sensing	Vector Network Analyzer
Sensitivity	7.3-9.5 dB	1.5-2.5 dB	10%	1.5-7 dB	3-9 dB	1.7-3.3 dB
Data post processing	Peak Detection	Peak detection	N/A	N/A	N/A	N/A
Specific fabric required	No	No	N/A	Yes	Yes	No
Measurement range (m)	N/A	1.5	1-1.5	0.5	4-4.5	1.6

Chapter 2: Circular Edge-Fed Microstrip Patch Antenna Design

2.1 Research Design

When it comes to microstrip antennas, there are two primary designs that are used extensively: rectangular and circular patches. Both of these shapes may be seen rather often. When it comes to aspects like as gain, beam location, and efficiency, each of these designs has a unique set of characteristics that set it apart from the others. In this thesis, we will be concentrating on the circular patch antenna since it has a number of characteristics that are unique to itself and shows potential for a variety of applications, one of which is the development of breathing monitoring devices.

A variety of crucial measures and materials are required for the design and construction of edge-fed patch antennas. In the manufacturing process, the antenna patch and feed network are commonly carved into a lightweight and compact substrate. The dielectric constant of the substrate has a significant impact on the antenna's resonance frequency, bandwidth, efficiency, and size, making it one of the most critical design considerations.

The feed point of an edge-fed patch antenna is situated on the patch's edge, thus the name. The feed point is not in the exact middle, as it would be in a center-fed arrangement. Due to its ease of use, low cost, and broad range of substrate compatibility, edge-fed designs are often used.

An edge-fed patch antenna uses a microstrip feed line connected to the patch's outside edge for its feeding mechanism. A quarter-wave transformer is often used in this feed line to maximize energy transmission to the antenna. Reflections and standing waves, both of which may diminish efficiency and cause damage, can be avoided with the right impedance matching.

The antenna's patch element functions like a resonant cavity. A cylindrical radiating slit reaches all the way from the patch's edge to the ground below. This slot is vital to the antenna's performance since it influences the radiation pattern and polarization. It is possible to tailor the slot's radiation properties by adjusting its size and shape.

During operation, the patch's effective diameter is increased by the bordering fields that surround it. Therefore, in an edge-fed design, the diameter of the half-wave patch is often

less than half the wavelength in the dielectric medium. As a result, we can get the same level of performance with a much smaller antenna.

The antenna's radiating properties are enhanced by the electric fringing fields. The antenna's emission is caused by these fields, which emerge at the patch's periphery. The patch's dimensions, shape, and material qualities, as well as the feed location and manner, all have a role in determining how they behave. To achieve the required radiation characteristics and best performance in certain applications, it is critical to understand and regulate these bordering fields.

These guidelines will be used to optimize the performance and functionality of a circular edge-fed linearly polarized patch antenna for respiratory monitoring systems. Careful consideration will be given to the substrate selection and preparation, patch and feed network design and placement, and fringing field management. The antenna's bandwidth and gain will be prioritized for development because of their importance to the antenna's overall performance and use in respiratory monitoring.

The basic drawing of a circular edge-fed patch antenna consists of the patch itself, a matching line, and a feeding line, as seen in the Figure 2.1.

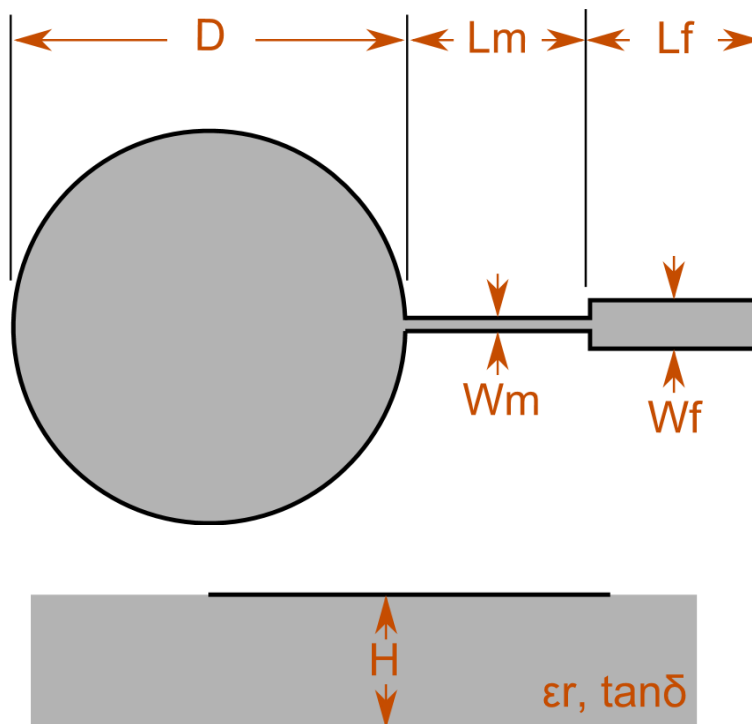


Figure 2.1: Basic drawing of a circular edge-fed patch antenna indicating the parameters

The antenna's radiating element is the circular patch. The size, shape, and material qualities of the substrate it is attached to determine the frequency at which it resonates. It is well-suited to a wide range of uses because to its round form, which permits distinctive emission patterns and polarization features. In addition, the edge-fed design simplifies production and implementation, providing a low-complexity, high-efficiency alternative to conventional, bulky antennas.

It is the matching line's responsibility to maximize the amount of energy transferred from the feeding line to the antenna. Typically, it takes the form of a quarter-wave transformer, a device that changes the impedance of the load such that it is identical to that of the source. The total performance of the antenna relies on the accuracy of the matching line's design and placement.

The electromagnetic waves are sent from the source to the antenna through the feeding line, also called a microstrip line. In an edge-fed arrangement, it's attached to the border of the circular patch, which simplifies manufacture and improves compatibility with integrated circuits.

The fabric or textile substrate in this design is one of the reasons why the antenna is so lightweight and adaptable. The design's adaptability is further enhanced by the usage of a material with future wearable technological uses.

The antenna's resonance frequency, bandwidth, and efficiency are all affected by the substrate's height 'h'. Broadband could be improved by using a thicker substrate, but efficiency and loss might suffer. Therefore, it is important to optimize the height of the substrate depending on the needs of the intended application while striking a balance between these opposing elements.

Circular microstrip antennas, distinguished by their round metallic overlays placed atop a dielectric foundation backed by a ground, are captivating in their design. A fascinating aspect is how the antenna's resonating frequency relates directly to its circumference. Given the radius, one can predict the operational frequency, which is essentially a function of the medium's wavelength. A myriad of radiation styles emanates from these antennas due to their potential to produce varying modes. Of these, the monopole and dipole modes stand out, influencing the emitted radiation signatures and polar orientations. The way power is introduced to the antenna, be it through a strip of

microchip, coaxial connectors, or other methods, has distinct ramifications on performance parameters such as matching impedance, radiation characteristics, and bandwidth. Speaking of bandwidth, while it tends to be on the narrower end for these antennas, strategic design maneuvers, like selecting a thicker foundation or adopting resonant structures, can stretch it. One cannot overlook the substrate's dielectric nature, as its constant not only dictates the overall size but also impacts the bandwidth. With the advent of the circular shape paired with the flexible nature of fabric-based backings, a myriad of innovative design opportunities beckon. This blend of attributes, together with the inherent adaptability of the antenna, hints at future explorations. From adapting to undulating structures to merging seamlessly with wearable devices and clothing, the horizon looks promising for these unique antennas [42]. As seen from equation (1), where f_o is the resonance frequency, c stands for the speed of light in a vacuum, a is the radius of the circular patch, and ϵ_{eff} is the effective dielectric constant. This equation establishes that the resonant frequency is inversely proportional to the radius of the patch and dependent on the effective dielectric constant of the substrate material. However, equation (2) is used to calculate ϵ_{eff} , such that the substrate's thickness h , ϵ_r is the relative permittivity of the material and d is the diameter of the circular patch. Whereas equation (3) is used to calculate the feedline width [42].

$$f_o = \frac{c}{2\pi a} \times \frac{1}{\sqrt{\epsilon_{eff}}} \quad (1)$$

$$\epsilon_{eff} = \frac{\epsilon_r + 1}{2} + \frac{\epsilon_r - 1}{2} \times \left[\frac{1}{\sqrt{1 + 12x \frac{h}{d}}} \right] \quad (2)$$

$$W_f = \frac{c}{2f_o \sqrt{\epsilon_{eff}}} \quad (3)$$

The feedline length doesn't generally follow a specific equation as the resonant frequency of the antenna is mostly dependent on the patch dimensions and not the feedline length. However, the feedline length can influence the input impedance and the matching.

In many designs, the feedline length is usually long enough to connect to external circuitry or to ensure that any mismatch is kept away from the main radiating structure. For inset-fed patch antennas, the inset depth (or length) is used to adjust the input impedance of the antenna. The design methodology for the proposed antenna is elucidated as follows: Initially, the resonant frequency was set at 2.4 GHz. Subsequently, the radius of the antenna was determined utilizing the equation:

$$r = \frac{F}{\sqrt{1 + \frac{2h}{\pi\epsilon_r F} \left(\ln \left(\frac{\pi F}{2h} \right) \right) + 1.7762}} \quad (4)$$

Here, h represents the height of the substrate, ϵ_r denotes the relative permittivity of the dielectric, and F is given by:

$$F = \frac{8.791 \times 10^9}{f_r \times \sqrt{\epsilon_r}} \quad (5)$$

In this context, f_r signifies the resonant frequency. The above equations yield an approximate value of 32.29 mm for the radius. However, adjustments were made based on parameter sweeps conducted in CST software. Moreover, the substrate height was ascertained by gauging the thickness of a T-shirt. The dimensions, length, and width of the substrate were derived as per the relation presented in [43]:

$$L = W = 2 \times \text{Patch diameter} \quad (6)$$

It should be emphasized that all parameters underwent fine-tuning using the parameter sweep functionality to derive the subsequent table of parameters presented below. Additionally, the feed line's length was approximated as the patch's radius, subject to further adjustments. Lastly, the variances observed in the inset feed length were influenced by the insights presented in [44].

Table 2: Proposed Antenna Parameters

Parameter	Value
Centre frequency	2.4 GHz
Feed line length	28 mm
Feed line width	1.9 mm
Patch diameter	62 mm
Relative permittivity	1.3
Substrate height	0.91 mm (2*0.455)
tan loss	0.0056
substrate width	126 mm (2*Patch Diameter)
substrate length	126 mm (2*Patch Diameter)
metal thickness	0.035 mm

The antenna characteristics utilized in the development of the circular edge-fed patch antenna for use in respiratory monitoring applications are listed in detail in Table 2. These values have been carefully chosen and tuned to get the best possible performance from the antenna. Table 2 provides essential guidance for the design process by outlining values that should be used to strike a good compromise between the many conflicting requirements of antenna design.

2.2 Design Using CST studio

Table 2 outlines the specifics of the suggested circular edge-fed patch antenna design, and this was realized with the use of state-of-the-art 3D electromagnetic (EM) modeling and analysis software, CST Studio Suite. Using this high-tech toolkit, we were able to simulate the antenna's behavior under a wide range of settings, adjusting and perfecting the design virtually before ever making a real prototype.

Extensive simulation, requiring several iterations and tweaks in a trial-and-error manner, defined the design process. Through many iterations, we were able to fine-tune the antenna's settings and arrive at a configuration that matched all of our requirements. These findings, which were attained by careful modeling and analysis, will be described at length in Chapter 3.

In order to better understand the antenna and its EM behavior under operating settings, the Figure 2.2 provides a sneak peek at the simulated antenna design as represented inside the CST Studio Suite environment.

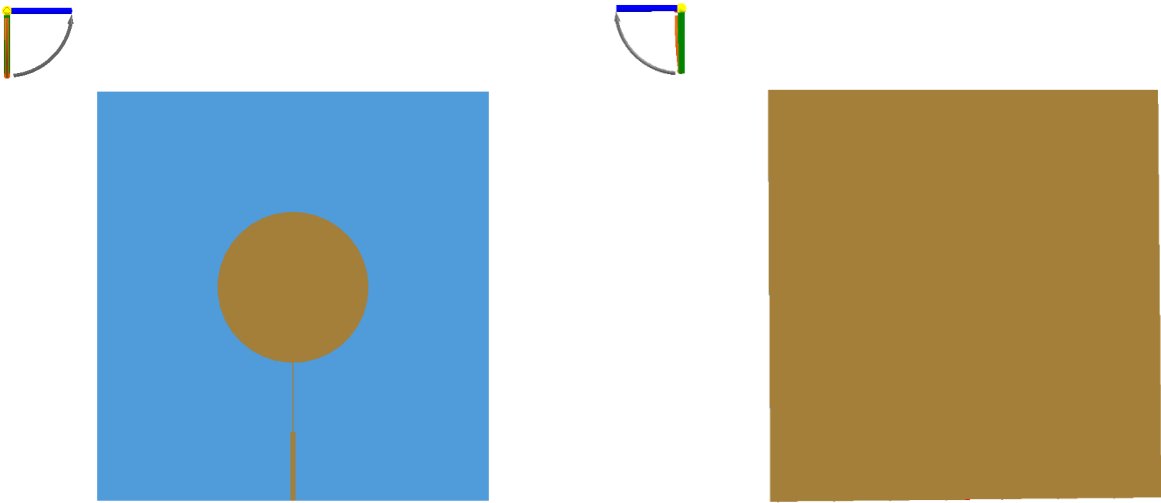


Figure 2.2: Circular edge-fed patch antenna using CST Studio software.

The production process was completed in China after extensive modeling and optimization, taking full use of the country's cutting-edge manufacturing capabilities and capacities. The actual antenna was delivered to the UAE after production was finished so that it could undergo testing and eventual deployment there. The constructed antenna is shown in Figure 2.3. With this prototype in hand, we've taken an important step toward our goal of creating a practical antenna for respiratory monitoring applications.



Figure 2.3: Circular edge-fed patch antenna final product

When it comes to the building of antennas, our design method optimizes the use of materials that are thin, lightweight, and flexible in order to bring a fresh creative viewpoint. An ultra-thin copper adhesive sheet with a thickness of just 0.035 millimeters was used in the antenna's design, which was done on purpose by our team. This small thickness guarantees that the antenna will have a low profile, which enables it to be smoothly integrated into applications that need inconspicuous integration, such as wearable technology.

In addition, the antenna is made to work on substrates made of textiles that have a thickness of up to 0.045 millimeters, which is an amazingly thin amount. The antenna's overall lightness and flexibility are increased because of the usage of such a thin substrate, which also adds to the antenna's overall lightness. This boosts the antenna's potential for use in wearable applications and small devices.

The relative permittivity of the textile material that was employed for the substrate was 1.3, which is noteworthy. This low permittivity value provides a benefit by lowering the velocity of propagation of electromagnetic waves, which may assist in miniaturizing the size of the antenna without sacrificing its performance. Additionally, it makes it possible for the antenna to function at higher frequencies, which expands the range of applications in which it may be used. Our work in the field of microstrip antenna development is distinguished by its innovative design and method, which aims to integrate high performance with lightweight and unobtrusive design. its novel design and method promise to make a substantial contribution to the improvement of wireless communication systems.

Chapter 3: Results and Discussions

As we go through this thesis, this chapter will illustrate and evaluate the results of the precise planning and rigorous simulation techniques covered. Using an ultra-thin copper adhesive sheet applied to a thin textile substrate, we have been primarily focused on constructing and studying a circular edge-fed patch antenna. Our mission is to completely redefine antenna construction for use in respiratory monitoring devices. In this section, we'll go through the simulation results we got from utilizing the CST Studio Suite, focusing on how the antenna performed in relation to its most important settings. In addition, we'll demonstrate the proposed antenna performance through measurements, critically comparing them to our theoretical forecasts. Our goal is to demonstrate the relevance of our research to the larger area of microstrip antenna design by a thorough analysis of these findings.

3.1 Design and Characteristics of the Microstrip Patch Antenna

As depicted in Figure 3.1, the circular patch antenna was meticulously designed and subsequently simulated utilizing the advanced capabilities of the CST Studio Suite software. The antenna was designed with certain measurements to make it work best for the frequency and purpose it was made for. The 2.4 GHz frequency has been picked as the antenna's center frequency. The length of the antenna's feed line is 28 mm, and its width is 1.9 mm. The spot on the antenna itself has a width of 62 mm. The relative permittivity of the surface on which the antenna patch is placed is 1.3. It has a height of 0.91 mm, which is almost twice as much as 0.455 mm. The loss of tan is written down as 0.0056. The width and length of the base are both 126 mm, which is the same as twice the diameter of the patch. Lastly, the metal used to make the antenna is only 0.035 mm thick.

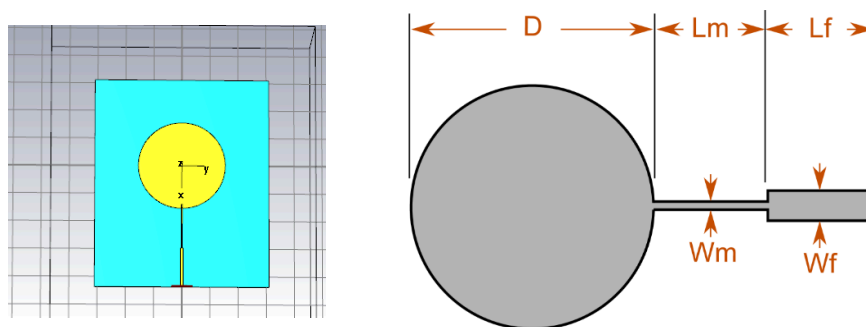


Figure 3.1: Circular edge-fed patch antenna design using CST

Figure 3.2 shows the S11 parameter (return loss) curve, which may be used to deduce important information about the resonant behavior of the anticipated antenna. If you find the spot on the S11 curve where the slope is at its lowest, that's the resonance frequency at which your antenna is most effective. As can be seen in the Figure below, our suggested antenna design has a resonance frequency of 2.4 GHz.

Understanding the significance of return loss, and especially S11, is important for both our present study and RF design as a whole. S-parameters tell us a lot about how the input and output ports of an electrical system work together. These factors are especially important in high frequency uses, where simple "open" or "closed" classifications of circuits no longer work. This is because things like parasitic capacitance, inductance, and the way transmission lines behave make things more complicated. Think of this idea as a ball being thrown against a wall. If the wall is completely solid, the ball will bounce back completely, like a strong RF wave. On the other hand, if it's a padded wall, the ball's energy is absorbed, which in RF terms is the same as minimum rebound. Here, the ball is the RF signal, the wall is the device, and the strength of the bounce-back is like S11.

Also, S11 isn't just about reflections; it's a key part of system design for matching resistance. The best case is when all of the power (the RF signal) that is sent to a device is consumed. This means that the impedance matches perfectly and the S11 number is close to zero. Real-world designs, on the other hand, often have problems with reflections, which makes S11 an important tool to measure and reduce these errors. Monitoring and improving S11 is a keyway to improve system performance, reduce the chance of signal confusion, and make sure that high-frequency processes go as planned.

An S11 value of -28.47 dB is achieved by the antenna at its resonance frequency as seen in Figure 3.2, indicating a very good impedance match with the typical 50 Ω transmission line. This optimal impedance matching ensures optimum power supply to the antenna for radiation while minimizing power reflection. An S11 value of -28.47 dB for a microstrip patch antenna is considered very good. The S11 parameter represents the return loss, which indicates how much of the input signal is reflected back from the antenna. The more negative the S11 value, the better, as it indicates less reflected power and more power being radiated by the antenna. Typically, in antenna design, an S11 value less than -10 dB is considered acceptable, as it means that 90% or more of the input power is accepted by

the antenna (and hence less than 10% is reflected back). A value of -28.47 dB indicates a very small amount of reflected power, signifying that the antenna is well-matched to its feedline and is operating efficiently at that particular frequency. So, our S11 value is not only considered high but is an excellent value, showcasing an efficient and well-matched antenna design.

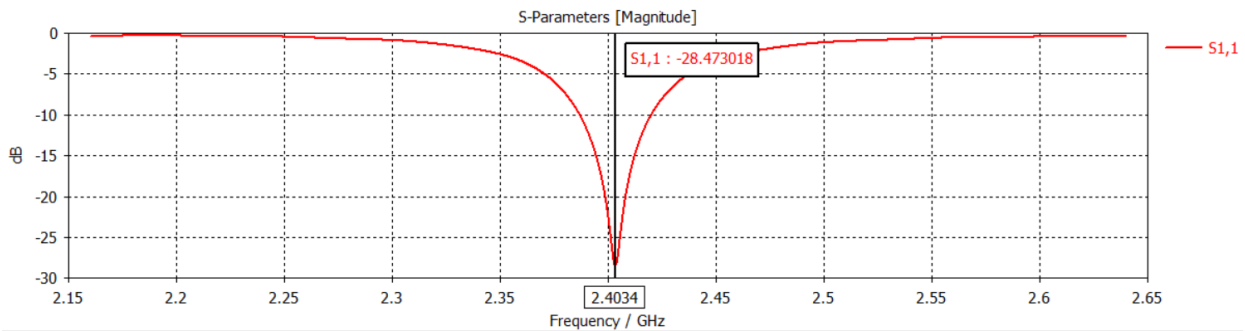


Figure 3.2: Simulated return loss (S11) for the circular patch antenna

In addition, the antenna's bandwidth is an essential performance characteristic that is normally calculated at the -10 dB return loss level on the S11 curve. This particular threshold is often used to represent a situation in which 90% of the input power is successfully received by the antenna, with just 10% being reflected back. This is a frequent scenario in which the antenna is employed in radio communications. We can get the antenna's bandwidth by finding the frequencies at which S11 hits -10 dB on the curve and then using the difference between these frequencies to compute the antenna's bandwidth. The bandwidth of our circular patch antenna may be determined by applying the following calculation:

$$BW = \frac{f_H - f_L}{\sqrt{(f_H \times f_L)}} \quad (7)$$

Which results in around 1.4%, as stated by [30] and can be seen in Figure 3.3. Comparatively, [31] notes that classic microstrip patch antennas are often narrow-band designs, with an impedance bandwidth that typically ranges from 1% to 2%. This is in contrast to the broad bandwidth offered by modern microstrip patch antennas. In light of this, the bandwidth of our antenna has the potential to be regarded as highly advantageous in the context of microstrip patch antennas.

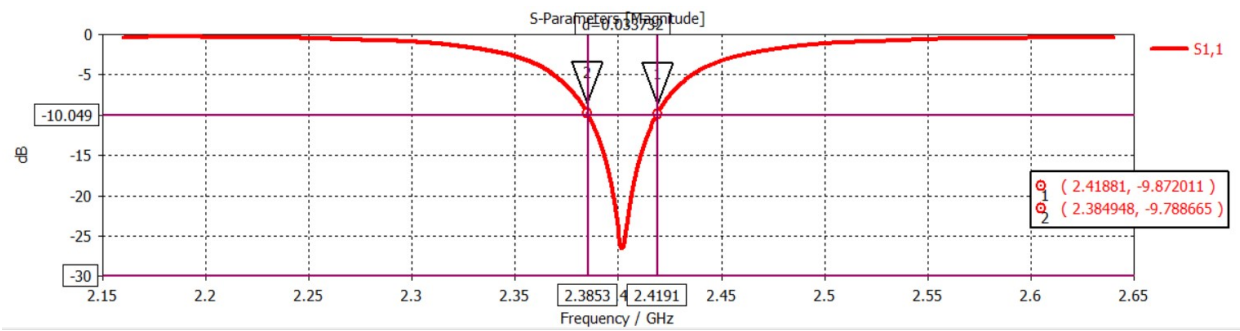


Figure 3.3: Simulated return loss (S11) for calculating the bandwidth of the circular patch antenna.

An essential statistic known as the voltage standing wave ratio (VSWR) assesses the impedance matching between an antenna and a transmission line or a source. It gives the ratio of the amplitude of the least voltage standing wave to the amplitude of the greatest voltage standing wave. According to [32], optimizing antenna performance requires keeping the voltage standing wave ratio (VSWR) as low as possible. This helps to guarantee that power is transferred effectively and reduces the likelihood of signal reflections. Figure 3.4 depicts the voltage standing wave ratio (VSWR) curve for the proposed antenna.

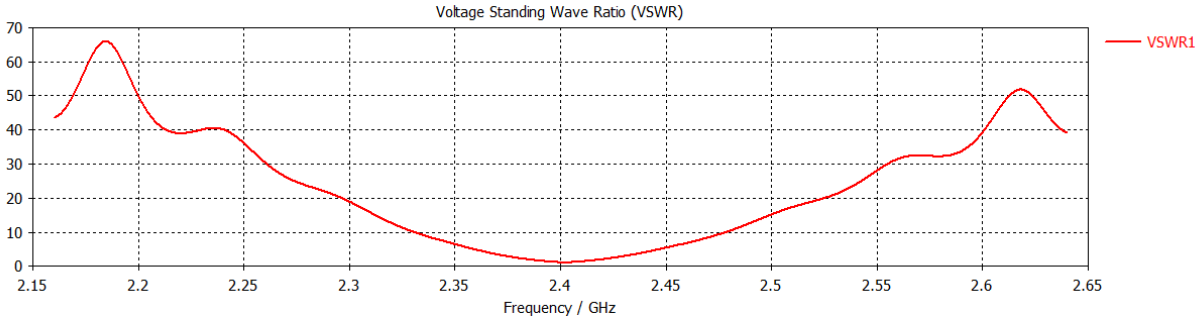


Figure 3.4: Simulated VSWR of the circular patch antenna

An important characteristic that determines how well an antenna radiates electromagnetic energy in a particular direction is called the "Realized Gain." It gives an indication of the amount of power that has been radiated in the intended direction, taking into account losses that have occurred owing to impedance and polarization mismatch. According to [33], maximizing signal intensity and enabling precision signal targeting

may be accomplished by achieving a high Realized Gain. Techniques for optimization include configuring antenna arrays, adjusting individual elements, and using beamforming algorithms. Figure 3.5 illustrates the realized gain that the suggested antenna has achieved in practice.

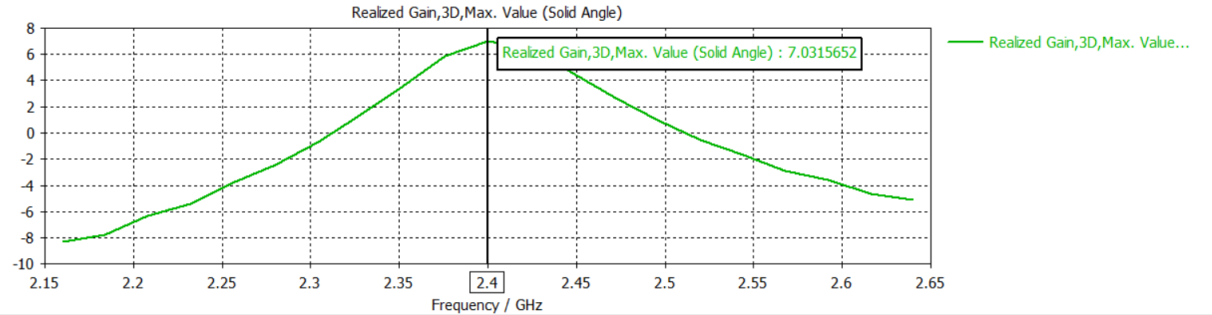


Figure 3.5: Simulated realized gain of the circular patch antenna.

When constructing an antenna, it is essential to take into account the efficiency of the antenna, which may be described as the ratio of the power that is coming into the power that is going out. Numerical representations of the input power and output power's respective % contributions to the antenna's overall power and the power it generates are provided. According to the findings of [34] study, an effective antenna decreases the amount of power that is lost while simultaneously enhancing signal intensity.

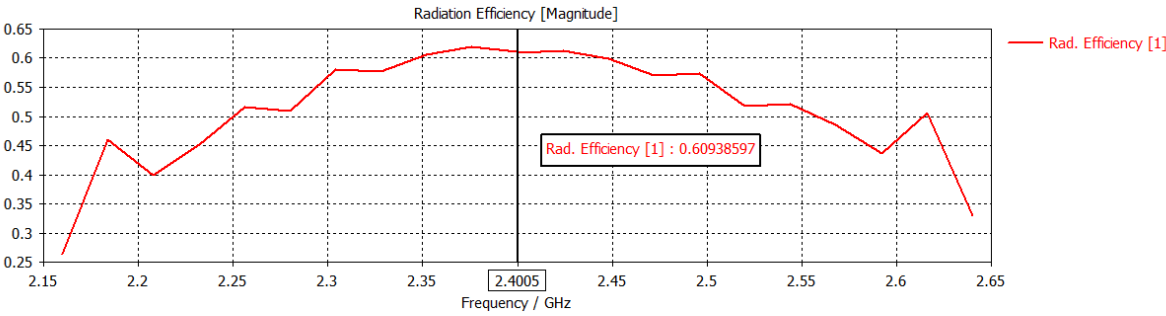


Figure 3.6: Simulated radiation efficiency of the circular patch antenna.

It is essential to keep in mind that the particular application and the performance criteria that are needed might have an effect on how appropriate the Efficiency rating is regarded to be. An efficiency of 61%, on the other hand, displays a noteworthy degree of

power conversion and may be deemed a beneficial outcome for the antenna's overall performance. This is because efficiency measures power conversion.

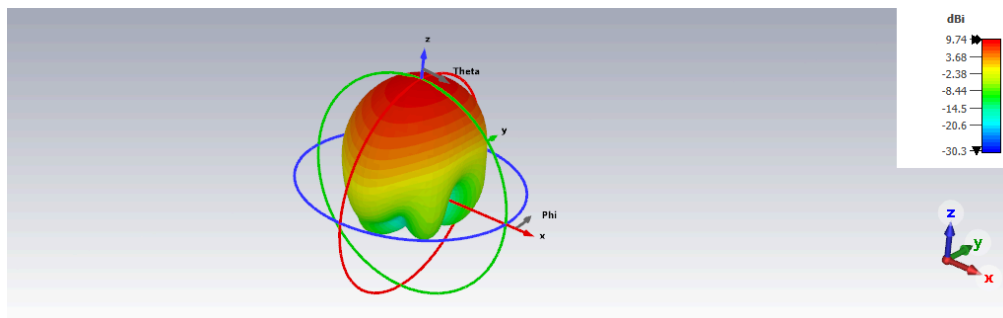


Figure 3.7: Simulated Far field of the circular patch antenna

The model proposed exhibits a uniform far-field radiation pattern, as shown in Figure 3.7. The maximum of the pattern is in a direction perpendicular to the plane in which the antenna is mounted; hence it is rather broad. [35] state that the geometry and impedance of the feed lines have the potential to influence the shape and directionality of the pattern, which in turn may impact the distribution of the radiated energy. The antenna's performance in a specific application may be improved by learning about and accounting for the impact of the feed-line network on the pattern of radiation.

3.2 Practical Microstrip Patch Antenna and Equipment Used

A very thin copper sheet with a thickness of 0.035 mm and an adhesive side was used to fabricate the proposed antenna. Due to its light weight and compact dimension, this ultrathin copper sheet is an ideal material for our applications. In addition, the antenna substrate was chosen to be a flexible textile material. This specific substrate option offers

both flexibility and durability, allowing the antenna to conform to a variety of shapes and surfaces while retaining its performance as you can see in Figure 3.8 below.



Figure 3.8: Circular patch antenna with stretchable textile substrate

Following assembly, a SMA connector must be soldered to the feeding line of the microstrip patch antenna, as seen in Figure 3.9. This prerequisite must be met before proceeding to the next stage.

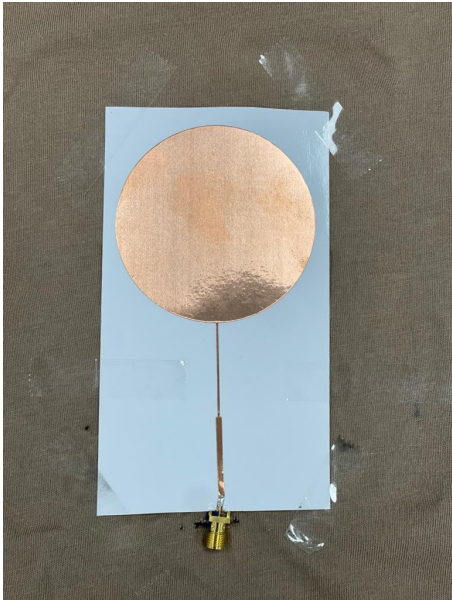


Figure 3.9: Circular patch antenna with stretchable textile substrate soldered to SMA connector

This SMA connection may be used as an interface between the manufactured antenna and the vector network analyzer (VNA). Once this link is established, the VNA can keep tabs on the antenna's impedance, return loss, and radiation pattern, among other characteristics. Since a SMA connector is used to link the antenna to the VNA, the antenna's performance may be thoroughly analyzed. Following these procedures, the antenna may be securely attached to the substrate by using the adhesive side. As can be seen in Figure 3.10, the antenna is reliably and securely attached to the substrate thanks to the adhesive layer.

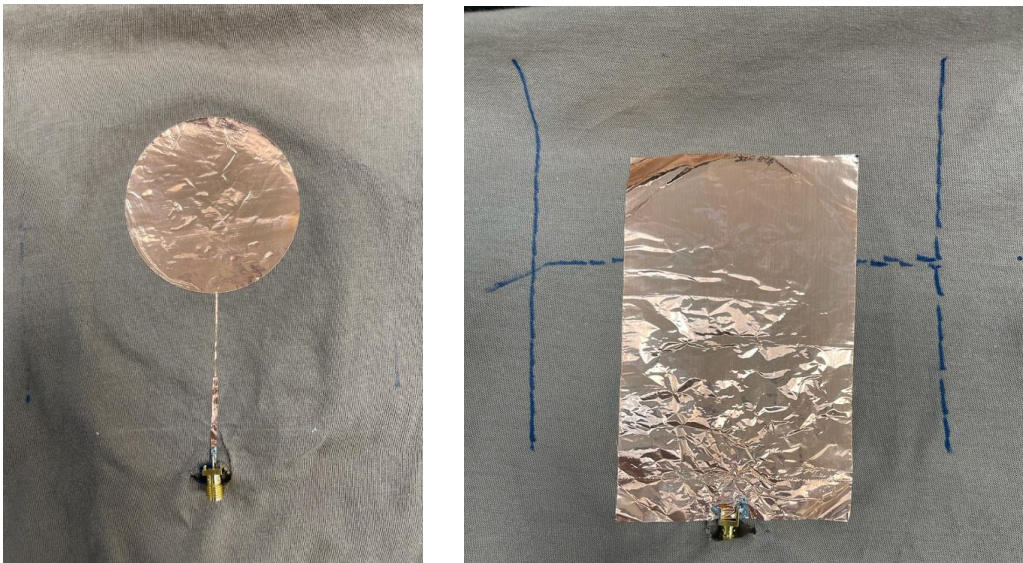


Figure 3.10: Circular patch antenna placed on the stretchable textile substrate along with the ground plane.

A ground copper plane is also attached to the substrate at the bottom. As can be seen in the same Figure, the ground plane acts as a point of reference for the antenna and contributes to its successful grounding and impedance characteristics.

The antenna's performance is analyzed using a Rohde and Schwarz ZVL13 Vector Network Analyzer (VNA) as seen in Figure 3.11.

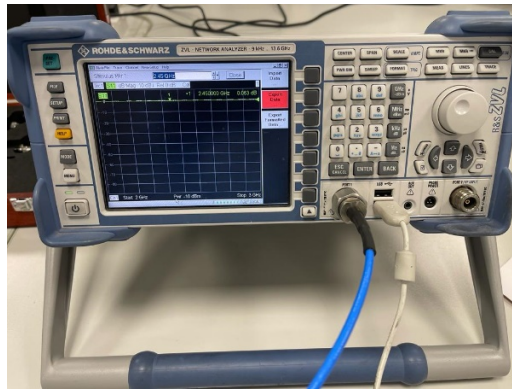


Figure 3.11: Rohde and Schwarz ZVL13 Vector Network Analyzer (VNA)

There is a three-stage calibration procedure performed on the VNA before it is used for measurements. One of these calibration procedures is called a Short-Open-Load (SOL) calibration, and it involves using short, open, and load standards as points of comparison for impedance matching. Next, a Through calibration is performed using a precision through adapter to account for any systematic errors caused by the transmission path. Finally, a Reflection calibration is executed to compensate for reflections at the VNA port by employing a calibrated reflection standard was done using the below equipment as you can see in Figure 3.12.



Figure 3.12: Rohde and Schwarz ZVL13 (VNA) calibration parts

3.3 Results of Different Breathing Patterns

Building upon the work reported in [36] and [37], our research team has recently been influential in the creation of a unique, non-invasive sensor built for contactless

monitoring of respiration rate. This sensor was developed to monitor respiration rate without making physical contact with the subject.

The diaphragm is largely responsible for contracting and relaxing in a rhythmic pattern throughout the process of human respiration. During the inhalation phase of breathing, a contraction of the diaphragm causes an expansion of the thoracic cavity. This expansion results in a drop in the pressure inside the thoracic cavity, which in turn causes the lungs to expand. On the other hand, during expiration, the muscles in the intercostal space and the diaphragm relax, which results in the chest and abdomen returning to their normal resting positions.

The capacity of our antenna design to detect in a flexible manner the chest motions associated with respiration is one of the defining characteristics that set it apart from other designs. The intensity of the detected signal is directly proportional to the amount of chest movement that has been measured, giving a quantitative measurement of the breathing pattern.

During a carefully arranged experiment, we were able to effectively capture the breathing signals of a male volunteer subjected to varied rates of respiration. It is essential to emphasize, for the sake of medical applications, that the identification of modifications in a patient's breathing pattern and respiration rate frequently bears higher clinical importance than the simple measurement of the respiration rate [38] and [39]. For example, the symptoms of a disorder known as respiratory distress may include considerable fluctuations in the patient's respiratory rate or continuous shallow breathing.

We were able to identify a broad spectrum of breathing patterns, ranging from slow to rapid by capitalizing on the sensitivity and accuracy of our antenna design. This allowed us to detect a wide range of breathing patterns. Our antenna design has a greater potential for use in important medical applications because of its capacity to recognize and discriminate between different rates of breathing. For systems monitoring breath via radio frequency methods, the reflection metric, commonly denoted as S_{11} , is pivotal. Its importance is underscored for numerous reasons.

Primarily, when S_{11} showcases an elevated gain, it implies the system can glean a potent reflection from subjects, like the human chest. This strength is pivotal as it dictates how finely we can interpret respiratory rhythms. Minute chest motions due to delicate

breaths or small hiccups in breathing are clearer with amplified gain, enriching the depth of analysis.

Further, distinguishing regular from atypical breathing becomes feasible with pronounced gain. Any slight variation in breathing can hint at looming health challenges. Elevated S11 gain ensures these subtle shifts don't go unnoticed, positioning the system as an essential health sentinel.

Additionally, elevated gain refines the signal-to-noise balance. This amplification ensures that breathing readings remain distinct, overshadowing potential disturbances. Such clarity is indispensable, especially in settings rife with interferences. Moreover, with amplified gain, consistency is ensured irrespective of the subject's activity level, be it deep rest, light activity, or intense exertion. This resilience is vital for 24/7 monitoring systems.

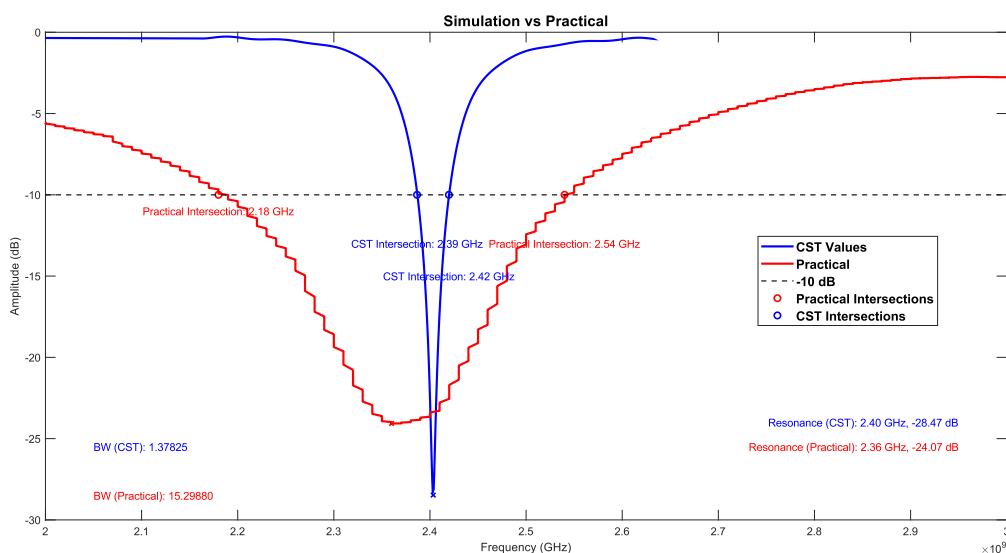


Figure 3.13: Return loss curve for simulated and practical antenna.

Upon comparison of the simulated and practical S11 characteristics of the proposed antenna, there are several noteworthy observations as seen in Figure 3.13. The simulated antenna yielded an S11 value of -28.47 dB at 2.4 GHz, boasting a bandwidth of 1.36%. In contrast, the practical measurements revealed an S11 value of -24 dB at a slightly shifted frequency of 2.36 GHz and a notably broader bandwidth of 15.28%. Although the practical S11 magnitude is slightly less ideal than the simulated value, it still offers excellent performance, well below the -10 dB threshold commonly sought after. The most

prominent distinction lies in the bandwidth; the practical antenna exhibits a considerably wider bandwidth compared to the simulation. This substantial bandwidth expansion in the real-world measurement is of significant interest, especially for microstrip patch antennas, where values above 5% are often labeled as "wideband".

This discrepancy between the simulated and actual outcomes may be attributable to a number of different variables. To begin, there is the possibility that the behavior of the antenna may be somewhat altered due to the existence of manufacturing tolerances and material qualities in the actual implementation. In addition, the performance of the antenna may be negatively impacted by electromagnetic interactions with the environment around it, such as those that occur with neighboring objects or buildings. In addition, impedance mismatches or inadequate connections in the actual configuration might potentially contribute to the variations that were found.

Multiple tests were performed to assess the antenna's typical functioning circumstances, with the exception of a specialized analysis of the breathing rate. Figure 3.14 depicts the S11 findings achieved for these trials. The average value of these trials was also calculated, and the matching curve was plotted. The average S11 value was found to be about -24 dB, with a frequency of operation of 2.36 GHz.

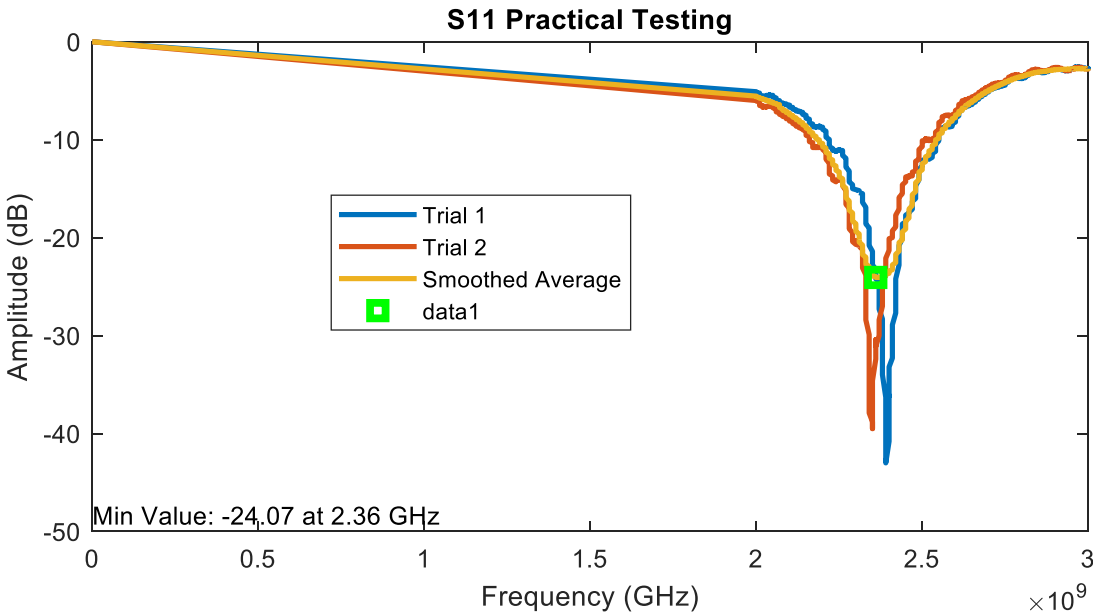


Figure 3.14: Return loss curve for multiple trials

These experimental studies give information about the antenna's performance under typical working settings, in addition to evaluating its usefulness in monitoring breathing rates. The average S11 value indicates the antenna's impedance matching, with a lower value suggesting better impedance matching and lesser power loss. Operating at 2.36 GHz implies a particular use or compatibility with a certain frequency range.

The next step involves placing the antenna on a volunteer's chest and running several tests to capture S11 curves during regular breathing. The information gathered will be utilized to determine how well the antenna functions under real-world conditions.

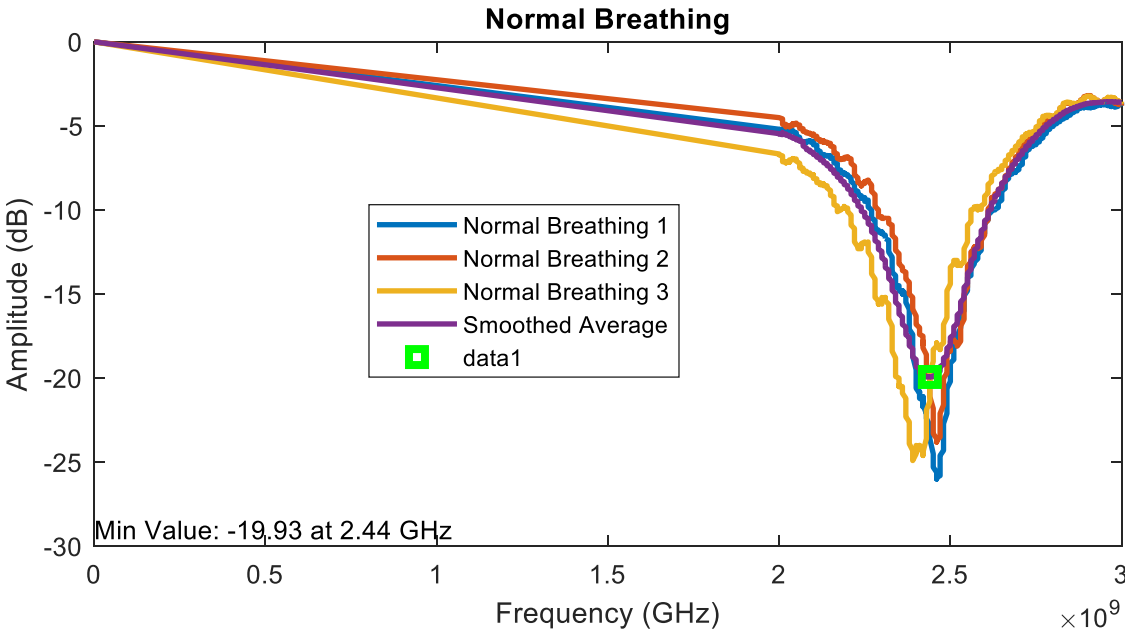


Figure 3.15: Return loss curve for multiple trials under normal breathing pattern

The acquired S11 curves for these trials are shown in Figure 3.15, along with the average curve, which represents the mean value throughout all trials. It was shown that 2.44 GHz is the optimal operating frequency for an average S11 of -20 db. This finding suggests a frequency change from the 2.36 GHz operating frequency. In Figure 3.16, we can investigate the phase variation with respect to normal breathing pattern.

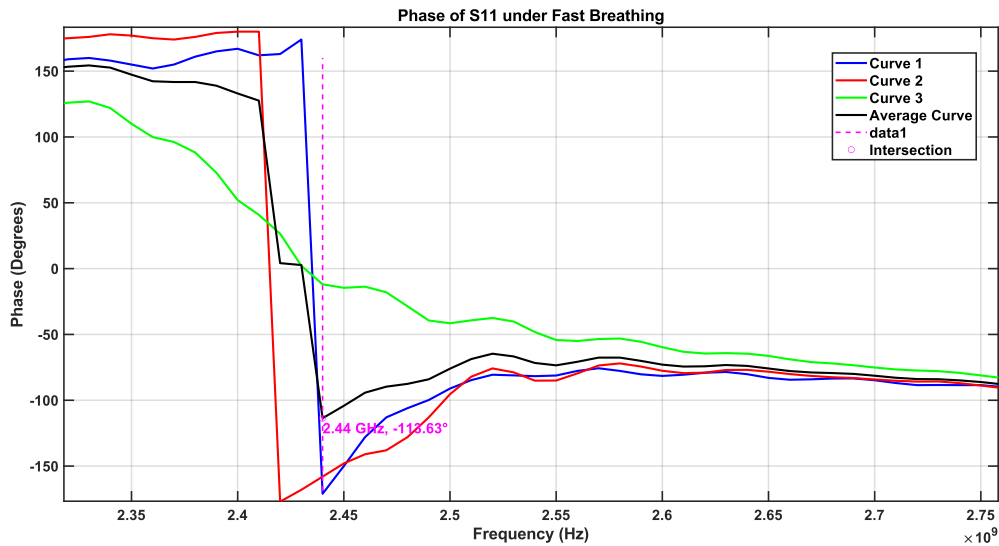


Figure 3.16: Return loss phase curve for multiple trials under normal breathing pattern

Table 3: S11 values under normal breathing pattern

Trial	S11 value (dB)	Frequency (GHz)
1	-25.9	2.46
2	-23.7	2.46
3	-24.9	2.39
Smoothed Average	-20	2.44

You can see in Table 3 the values of the S11 and the frequency shift that happened during normal breathing pattern. The resonance frequency of the antenna may be affected by the breathing motion and accompanying chest wall motions, resulting to the observed frequency change when the antenna is placed on the chest of a volunteer.

For the slow breathing scenario, a series of multiple trials will be conducted to record the S11 curves. These trials aim to capture the antenna's performance during slow breathing patterns. The collected data is presented in Table 4, providing detailed insights into the variations observed across the different trials.

Table 4: S11 values under slow breathing pattern

Trial	S11 value (dB)	Frequency (GHz)
1	-17.7	2.47
2	-21.7	2.42
3	-21.5	2.44
Smoothed Average	-17.4	2.43

Moreover, the average of these S11 curves is calculated and plotted to gain a comprehensive understanding of the overall performance as in Figure 3.17. The average S11 value obtained from the slow breathing trials is approximately -17.4 dB, with a corresponding frequency of operation at 2.43 GHz. It is noteworthy to observe a frequency shift from the original working frequency of 2.36 GHz. Also Figure 3.18 presents the phase variations under slow breathing pattern.

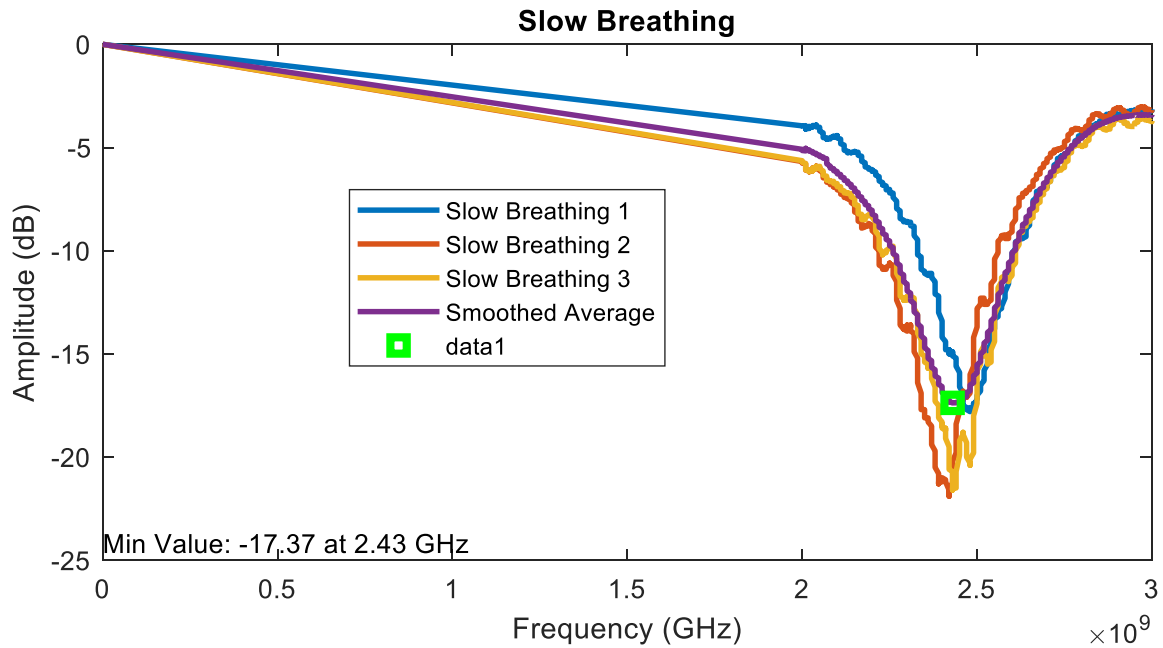


Figure 3.17: Return loss curve for multiple trials under slow breathing pattern

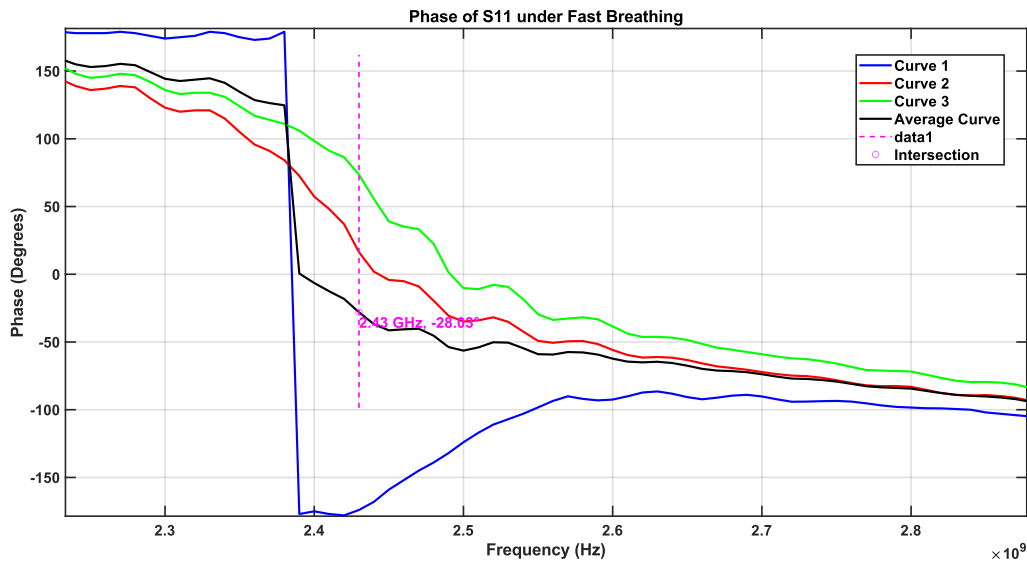


Figure 3.18: Return loss phase curve for multiple trials under slow breathing pattern

In order to assess the antenna's performance during fast breathing, a series of multiple trials will be conducted, capturing the S11 curves in this specific scenario. The recorded data can be found in Table 5, providing detailed information regarding the observed variations across the different trials.

Table 5: S11 values under fast breathing pattern

Trial	S11 value (dB)	Frequency (GHz)
1	-28.8	2.44
2	-28.3	2.48
3	-21.3	2.49
Smoothed Average	-20.5	2.47

Moreover, the average S11 curve is computed and plotted to provide a comprehensive overview of the overall performance as in Figure 3.19. The average S11 value obtained from the fast-breathing trials is -20.5 dB, with a corresponding frequency of operation at 2.47 GHz. Notably, a frequency shift is observed from the original working frequency of 2.36 GHz. In addition, Figure 3.20 presents the phase variations under fast breathing.

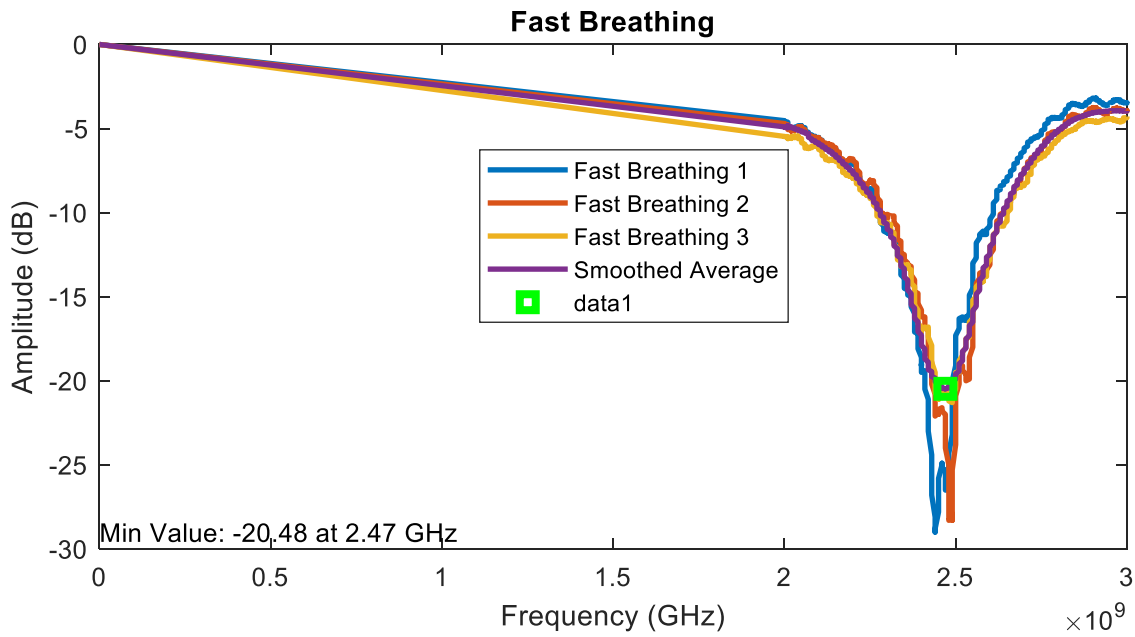


Figure 3.19: Return loss curve for multiple trials under fast breathing pattern

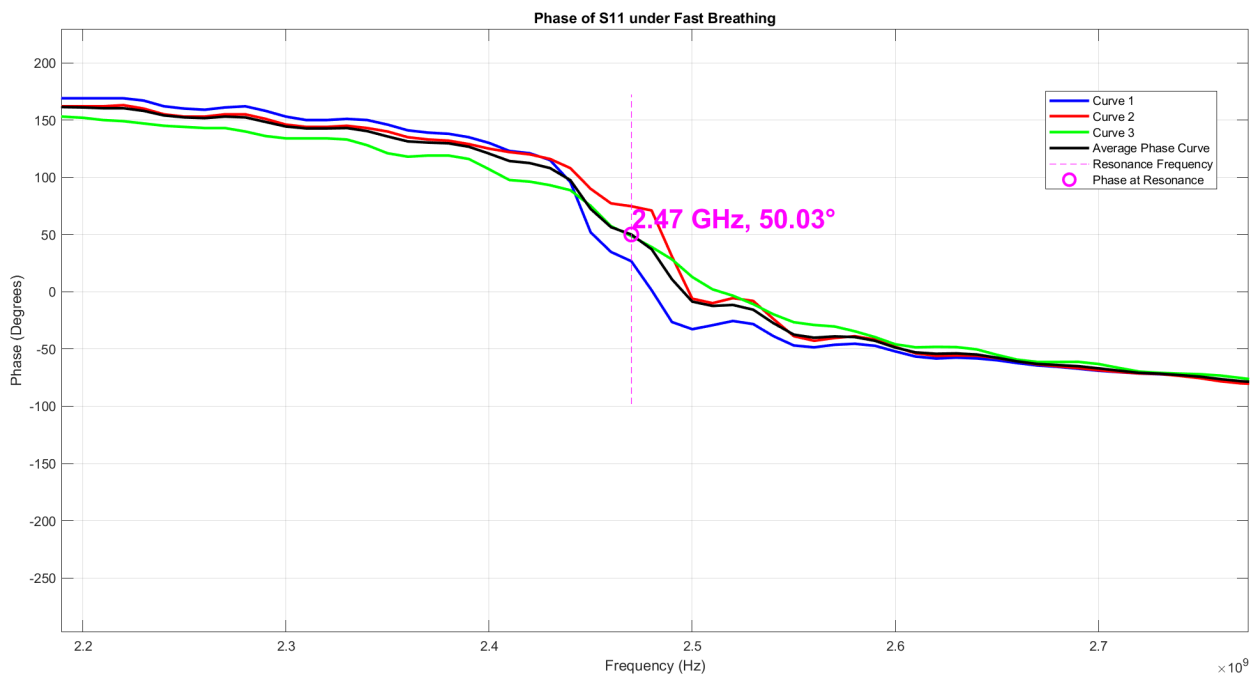


Figure 3.20: Return loss phase curve for multiple trials under fast breathing pattern

Figure 3.21 represents a comparison between different breathing pattern averages and no breathing curve.

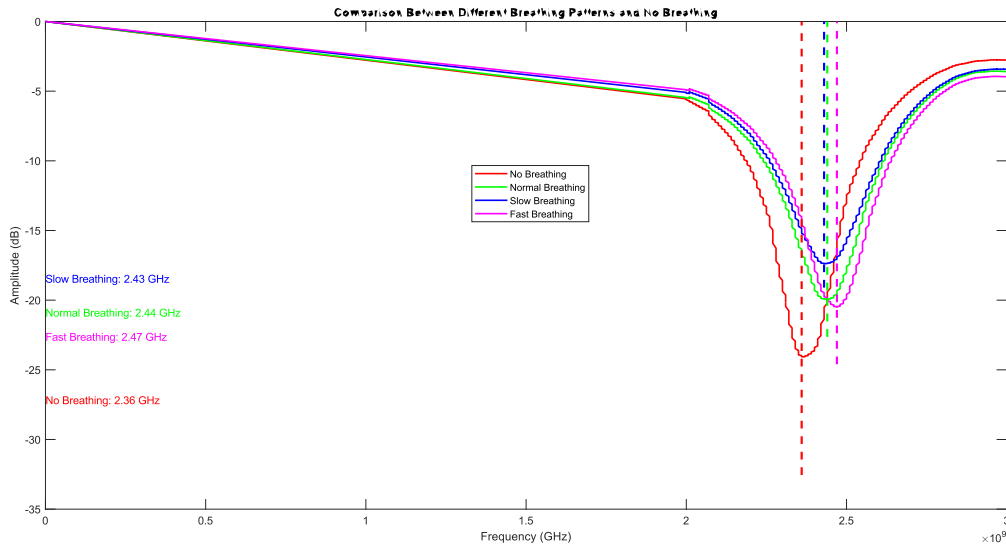


Figure 3.21: Return loss curves comparison between different breathing patterns and no breathing

From Figure 3.21, the distinction and phase shift among the curves is evident. Using the "no breathing" curve operating at 2.36 GHz as a reference, we observe shifts for slow breathing to 2.43 GHz, normal breathing to 2.44 GHz, and fast breathing to 2.47 GHz.

3.4 Breathing Rate Estimation

To accurately estimate the breathing cycle from the interactions with a monitored entity, a meticulous procedure was followed, anchored on the analysis of the dBm of the Inverse Fast Fourier Transform (IFFT).

Initially, the dataset was sorted by frequency to establish a logical sequence crucial for further operations such as smoothing and Fourier transformations. This foundational step eliminated the possibility of potential miscalculations due to disordering.

Next, duplicate frequencies, which could distort the interpretative process by overweighing certain data points, were meticulously removed. This ensured that the evaluation was based on unique, unbiased data points, laying the groundwork for accurate interpretations. The data then underwent a smoothing process to counteract minor fluctuations and potential high-frequency noise, ensuring a clearer, more consistent representation of broader trends. This process becomes indispensable when aiming to pinpoint significant features like resonance frequencies. Identification of the resonance frequency was crucial in this sequence. It's the frequency at which the system is most

resonant, typically discernible where the magnitude of reflection (S11) is at its lowest. Pinpointing this minimum magnitude opened the door to understanding the system's intrinsic behavior. Merging the magnitude and phase of the signal through the Complex S11 calculation was vital. This comprehensive representation was essential to transition from frequency domain data to time domain through IFFT, revealing otherwise hidden time-based patterns. At this juncture, it's worth noting that the direct IFFT curve was initially inspected. The purpose of this operation is to convert the frequency domain data back to the time domain. In the context of MATLAB (which the code is written in), this operation is efficiently handled by the `ifft` function. Mathematically, the IFFT can be described by the formula:

$$s_{11_time} [n] = \frac{1}{N} \sum_{k=0}^{N-1} S_{11_complex} [k] \cdot e^{j\left(\frac{2\pi}{N}\right)kn} \quad (8)$$

Here:

- N is the time index.
- N is the total number of data points
- S11 complex [k] is the complex representation of S11 in the frequency domain for a specific frequency index k.
- J represents the imaginary unit

However, it didn't yield significant or clear information regarding the breathing cycles. This led to the decision to focus on the dBm of the IFFT. The dBm, which represents power levels in decibels relative to one milliwatt, showcased variations and patterns more distinctly than the IFFT curve alone.

$$dBm = -10 \times \log_{10}(|s_{11_time}|) \quad (9)$$

Here, S11 time is the result of the IFFT.

These fluctuations were presumed to correspond to breathing-induced interactions with the monitored system.

Upon examination of the dBm of the IFFT, a trough-peak-trough detection algorithm was implemented to decipher the breathing patterns. Peaks and troughs, which became evident, were interpreted as signals for breathing cycles. To determine the breathing rate, it was postulated that the breathing cycle for each pattern would be

relatively consistent over a span of one minute. Based on this assumption, it became feasible to calculate the average breathing rate in Breaths per Minute (Bpm). In essence, this method integrated rigorous data processing with insightful assumptions and analytical techniques. The systematic processing of the dBm of the IFFT, combined with the application of specialized algorithms, made it possible to detect and interpret biological patterns, such as breathing, effectively. This endeavor underscores the significance of adopting a multi-faceted approach to unveil subtle physiological patterns that might otherwise remain concealed.

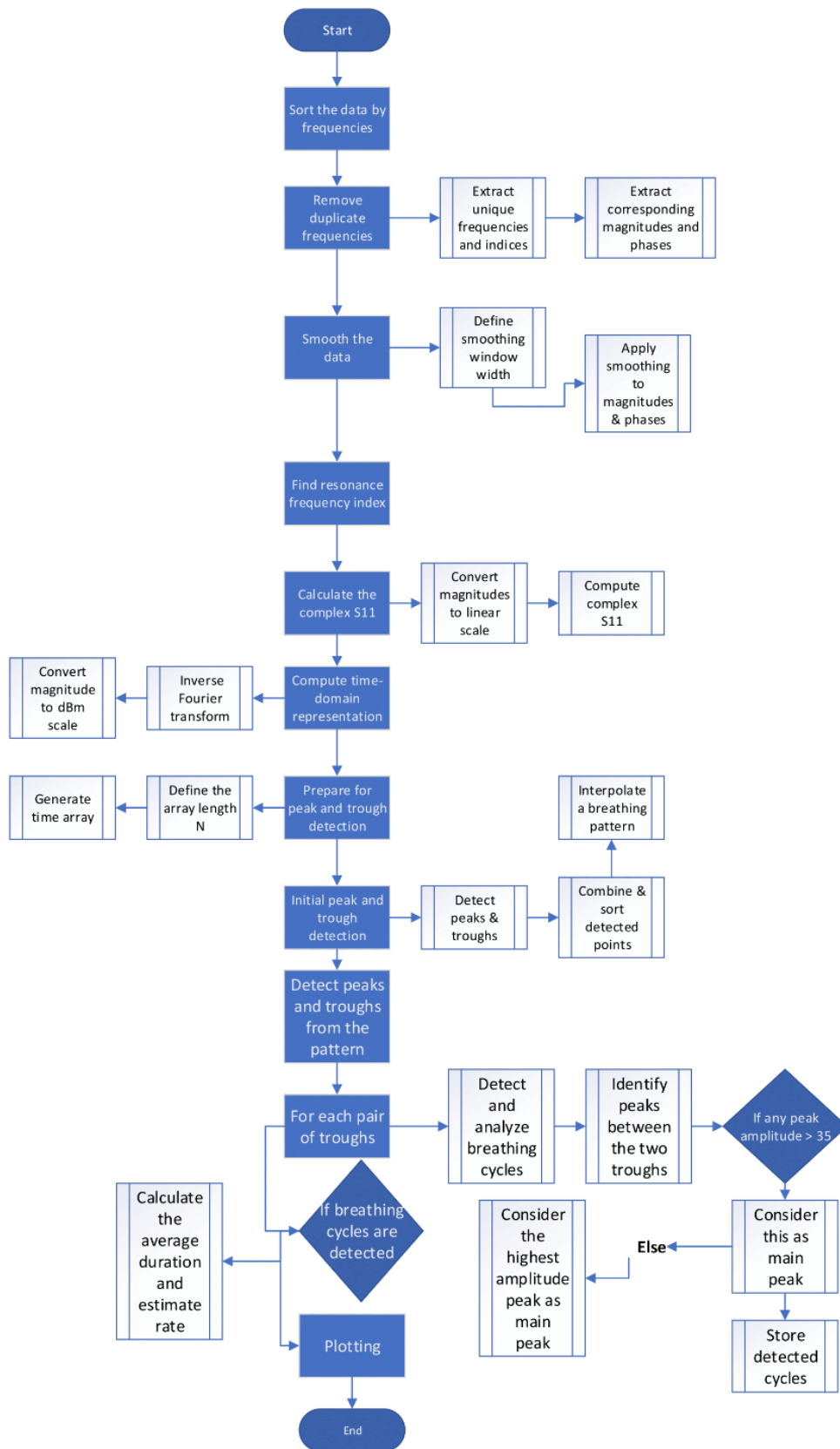


Figure 3.22: Flowchart of the Breathing Rate Estimation Process

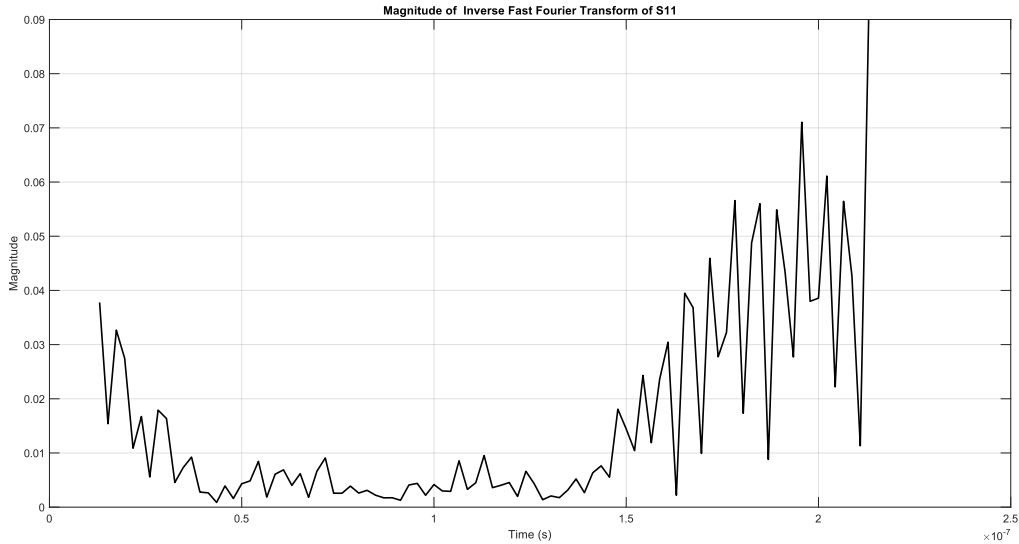


Figure 3.23: Magnitude of IFFT of S11 under normal breathing

From Figure 3.23, it is evident that there are fluctuations in the data. However, these do not accurately represent the genuine breathing pattern. In contrast, Figure 3.24 clearly depicts the breathing cycles. The process starts by identifying distinct breathing cycles based on the troughs and peaks in the dBm curve values. Each of these cycles represents a complete breath, encompassing an inhalation and an exhalation. From these detected cycles, the time durations for individual breaths are computed. The average time taken for one complete breath is then determined by calculating the mean of these durations. This average duration is pivotal as it provides the time taken for a single inhalation-exhalation cycle. To convert this average time into a breathing rate, the code takes the reciprocal of the duration (i.e., how many breaths would occur in a unit of time) and scales it to obtain the rate in terms of breaths per minute (Bpm). This rate, presented in Bpm, offers a clear understanding of respiratory activity, which is invaluable for assessing health and potential respiratory anomalies. The breathing rate can be determined using the formula:

$$\text{Breathing rate} = \frac{60 \text{ seconds}}{\text{mean (breathing duration)}} \quad (10)$$

Here, the breathing duration is determined by computing the time difference between a peak and its subsequent trough.

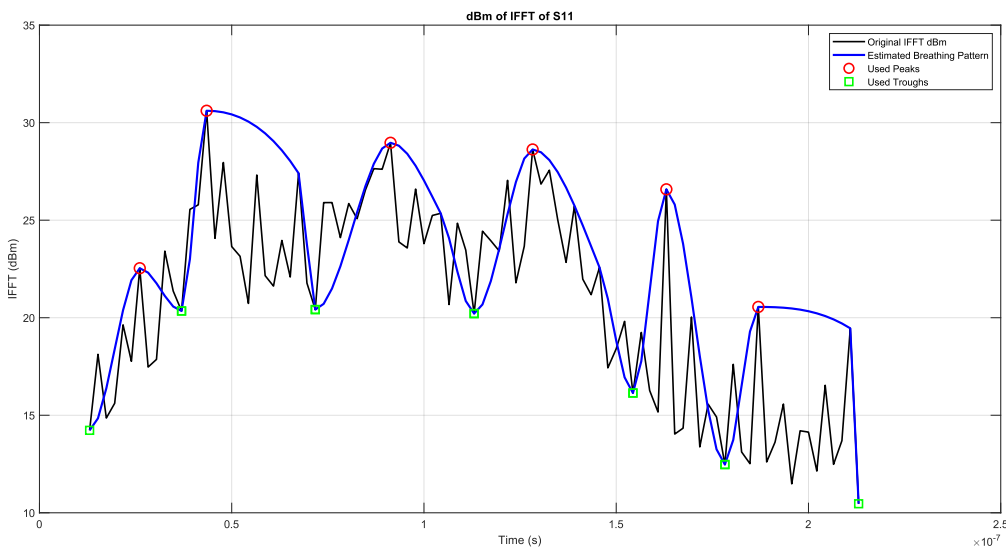


Figure 3.24: Magnitude of dBm of IFFT of S11 under normal breathing

By employing the aforementioned methodology to estimate the breathing rate in Bpm, a rate of 18 Bpm was determined for an individual exhibiting a standard breathing pattern. According to medical literature, the typical respiratory rate for adults' ranges between 12–18 bpm [40]. Figure 3.25 presents the IFFT curve under fast breathing as well as Figure 3.26 presents the dBm of the IFFT of S11 under the same breathing pattern. We can observe a breathing rate of 22 Bpm. This elevated rate is well above the typical adult rapid respiratory rate above 20 bpm as stated in medical literature [40].

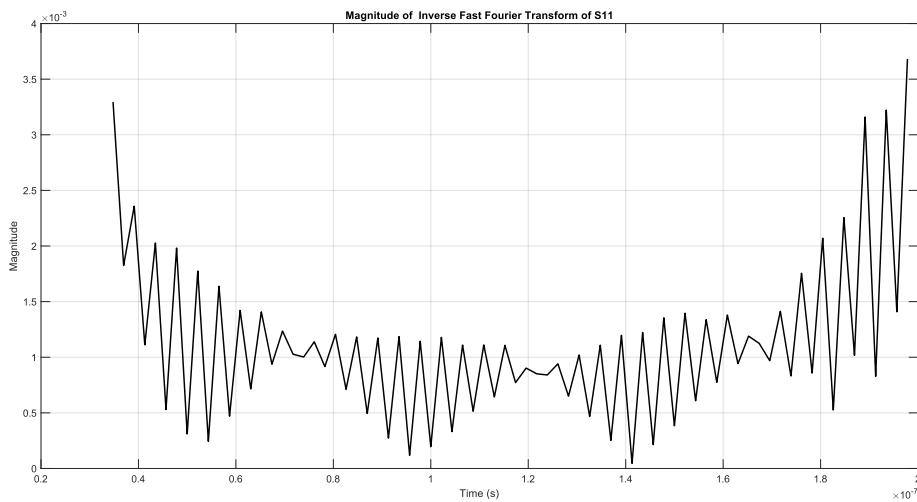


Figure 3.25: Magnitude of IFFT of S11 under fast breathing

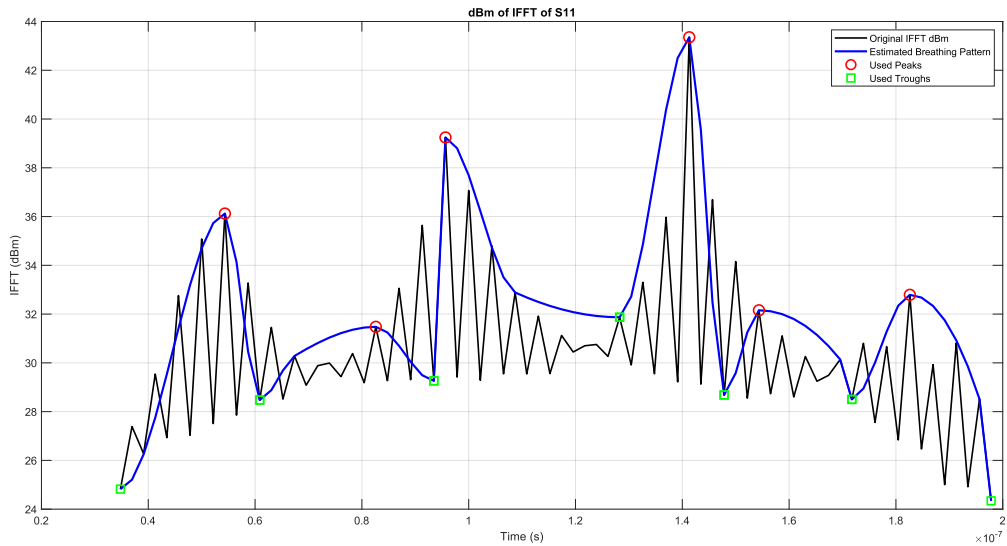


Figure 3.26: Magnitude of dBm of IFFT of S11 under fast breathing

Figure 3.27 displays the IFFT curve corresponding to a specific breathing pattern, while Figure 3.28 showcases the dBm of the IFFT of S11 for the same conditions. An observed breathing rate of 14.7 Bpm is evident. This rate is consistent with typical respiratory rates in adults, as referenced in medical literature [40].

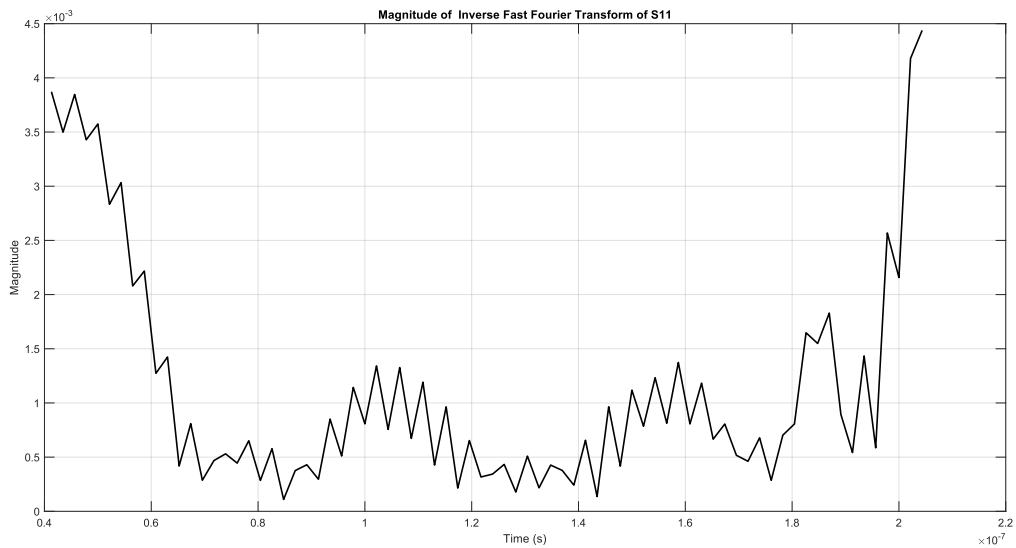


Figure 3.27: Magnitude of IFFT of S11 under slow breathing

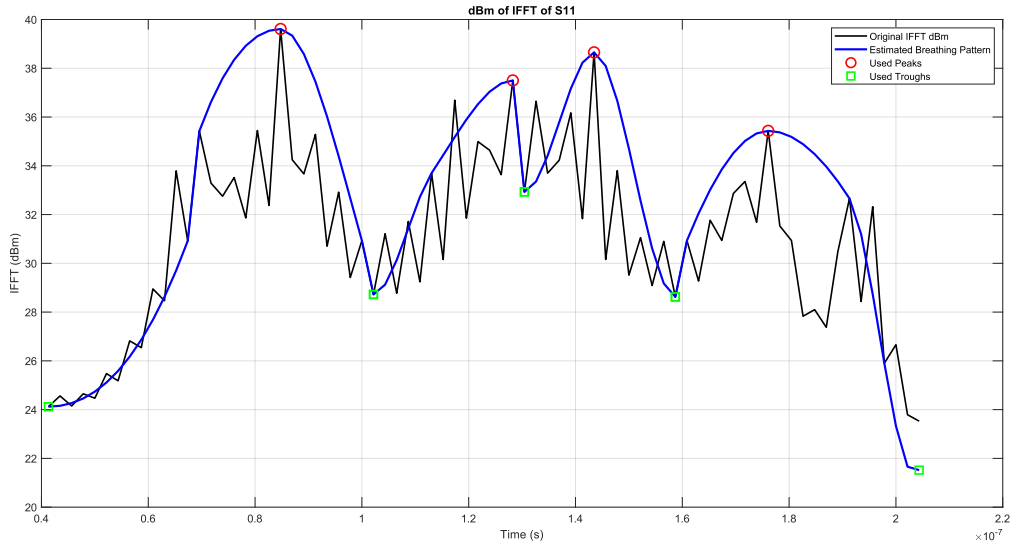


Figure 3.28: Magnitude of dBm of IFFT of S11 under fast breathing

Table 6: Summary of different breathing pattern in terms of frequency, S11, Phase and Breathing rate

Pattern	Frequency (GHz)	S11 value (dB)	Phase (degrees)	Breathing rate (Bpm)	Medical reference (Bpm) [40]
Normal	2.44	-20	-113.63	18	12-18
Fast	2.47	-20.5	50.03	22	20 < bpm
Slow	2.43	-17.4	-28.03	14.7	9-14

Table 6 presents a summarized view of different breathing patterns, capturing the distinct characteristics associated with each pattern in terms of frequency, reflection coefficient (S11), phase, and breathing rate. For a normal breathing pattern, the frequency is 2.44 GHz, the S11 value stands at -20 dB, and the phase is -113.63 degrees, leading to a breathing rate of 18 Bpm, which aligns with the medical reference range of 12-18 Bpm as noted in [40]. The fast-breathing pattern, with its frequency at 2.47 GHz, reflects an S11 value of -20.5 dB and a phase of 50.03 degrees, correlating to a breathing rate of 22 Bpm. This rate surpasses the medical reference of anything greater than 20 Bpm. In contrast, the slow breathing pattern is characterized by a frequency of 2.43 GHz, an S11

value of -17.4 dB, and a phase of -28.03 degrees. Its breathing rate is 14.7 Bpm, fitting within the medical reference of 9-14 Bpm.

Chapter 4: Conclusion

In this chapter, we draw together the significant findings from our research and explore their wide-ranging implications, touching on the managerial implications relevant to healthcare and wearable technology sectors as well as the broader scientific contributions our research provides.

4.1 Managerial Implications

Significant management implications come from our investigation into the design and implementation of a circular edge-fed patch antenna for use in respiratory monitoring systems. The revolutionary potential of this antenna lies in the fields of healthcare, wearable technology, and remote patient monitoring due to its capacity to function with textile materials of low thickness and relative permittivity of 1.3.

The ability of our antenna system to properly discern between different breathing rates is one of its defining features. In our experiments, we were able to accurately identify and categorize breathing rates from rapid 22 Bpm to normal 18 Bpm to slow 14 Bpm. Early diagnosis and treatment of health issues made possible by such sophisticated monitoring might greatly enhance patient outcomes while also possibly lowering healthcare expenditures.

From a business perspective, our results indicate there is a chance to incorporate such antenna technology into wearable devices, providing a considerable competitive advantage. Wearable gadgets using our cutting-edge respiratory monitoring might address a growing need as public interest in personal health monitoring grows.

4.2 Research Implications

Our recent investigations into antenna design for respiratory monitoring have unveiled findings of considerable significance, drawing on a structured approach to data analysis. This structure, underpinned by a methodical flowchart, serves as the foundation for our research, guiding us through a comprehensive exploration of the data and its nuances.

Beginning with the data at hand, the initial stages (Steps 1 and 2) revolved around sorting the data by frequencies and removing any duplicate frequencies. These stages ensured the integrity of our data and set the stage for subsequent steps by extracting unique

frequencies, alongside their corresponding magnitudes and phases. Having cleaned our data, we proceeded to the essential process of data smoothing (Step 3), which involved defining a smoothing window width and subsequently applying this smoothing to both magnitudes and phases. This was pivotal in enhancing the clarity of our data and preparing it for the following analysis. Steps 4 through 6 delved deeper into the intricacies of our dataset. We identified the resonance frequency index. The culmination of this segment was the calculation of the complex S11, wherein magnitudes were converted to a linear scale. Transitioning into the realm of time-domain representation (Step 7), our research leveraged the Inverse Fourier transform to convert magnitudes to the dBm scale. This was followed by a rigorous process of peak and trough detection (Steps 8-11), where we meticulously defined array lengths, generated time arrays, and detected peaks and troughs, before interpolating a breathing pattern. With these patterns in hand, the subsequent steps (Steps 12 and 13) facilitated a deep dive into analyzing breathing cycles between troughs and estimating the rate of breathing. It was in these stages that the potential of our method truly shone, offering insights into real-world problems like discerning varying breathing rates.

4.3 Research Limitations

In the exploration of the antenna tailored for breathing pattern discernment, certain restrictions have come to the fore. Its design specificity at 2.4 GHz narrows its operational sphere primarily to this designated frequency, potentially curtailing its utility for multi-frequency applications. Its physical size could prove cumbersome for specific use cases, especially when considering integration into wearable devices where sleekness is vital. Of significant concern is the antenna's potential vulnerability to environmental factors, such as interference from electronic devices or physical barriers.

4.4 Future work and Improvements

Several potential enhancements can be projected. Considering a design with a larger bandwidth could broaden its applicability, ensuring it operates over diverse frequency zones. A shift to a more streamlined shape, without compromising efficiency, might cater to wearable tech preferences. Advancing its precision in breathing pattern recognition through advanced algorithms can further its utility.

References

- [1] M. Venkatesan *et al.*, “Evolution of electrospun nanofibers fluorescent and colorimetric sensors for environmental toxicants, pH, temperature, and cancer cells – A review with insights on applications,” *Chemical Engineering Journal*, vol. 397, p. 125431, Oct. 2020, doi: 10.1016/j.cej.2020.125431.
- [2] I. Gagnadre, C. Gagnadre, and J. P. Fenelon, “Circular patch antenna sensor for moisture content measurement on dielectric material,” *Electronics Letters*, vol. 31, no. 14, p. 1167, Jul. 1995, doi: 10.1049/el:19950801.
- [3] F. Pozo, D. A. Tibaduiza, and Y. Vidal, “Sensors for Structural Health Monitoring and Condition Monitoring,” *Sensors*, vol. 21, no. 5, p. 1558, Feb. 2021, doi: 10.3390/s21051558.
- [4] C. Hertleer, H. Rogier, L. Vallozzi, and F. Declercq, “A textile antenna based on high-performance fabrics,” *European Conference on Antennas and Propagation*, Jan. 2007, doi: 10.1049/ic.2007.1085.
- [5] S. Saha *et al.*, “A Glucose Sensing System Based on Transmission Measurements at Millimetre Waves using Micro strip Patch Antennas,” *Scientific Reports*, vol. 7, no. 1, Jul. 2017, doi: 10.1038/s41598-017-06926-1.
- [6] H. Huang, “Flexible Wireless Antenna Sensor: A Review,” *IEEE Sensors Journal*, vol. 13, no. 10, pp. 3865–3872, Jan. 2013, doi: 10.1109/jsen.2013.2242464.
- [7] K. N. Paracha, S. K. A. Rahim, P. J. Soh, and M. Khalily, “Wearable Antennas: A Review of Materials, Structures, and Innovative Features for Autonomous Communication and Sensing,” *IEEE Access*, vol. 7, pp. 56694–56712, Apr. 2019, doi: 10.1109/access.2019.2909146.
- [8] M. T. Islam, Md. N. Rahman, M. Singh, and Md. Samsuzzaman, “Detection of Salt and Sugar Contents in Water on the Basis of Dielectric Properties Using Microstrip Antenna-Based Sensor,” *IEEE Access*, vol. 6, pp. 4118–4126, Jan. 2018, doi: 10.1109/access.2017.2787689.
- [9] M. Ridao-López, M. Comendheiro-Maaløe, N. Martínez-Lizaga, and E. Bernal-Delgado, “Evolution of public hospitals expenditure by healthcare area in the Spanish National Health System: the determinants to pay attention to,” *BMC Health Services Research*, vol. 18, no. 1, Sep. 2018, doi: 10.1186/s12913-018-3445-7.
- [10] H. Fouad, A. S. Hassanein, A. M. Soliman, and H. Al-Feel, “Analyzing patient health information based on IoT sensor with AI for improving patient assistance in the future direction,” *Measurement*, vol. 159, p. 107757, Jul. 2020, doi: 10.1016/j.measurement.2020.107757.

- [11] L. Maurya, P. Kaur, D. Chawla, and P. K. Mahapatra, “Non-contact breathing rate monitoring in newborns: A review,” *Computers in Biology and Medicine*, vol. 132, p. 104321, Mar. 2021, doi: 10.1016/j.compbiomed.2021.104321.
- [12] L. Gao, G. Zhang, B. Yu, Z. Qiao, and J. Wang, “Wearable human motion posture capture and medical health monitoring based on wireless sensor networks,” *Measurement*, vol. 166, p. 108252, Dec. 2020, doi: 10.1016/j.measurement.2020.108252.
- [13] M. Folke, L. Cernerud, M. Ekström, and B. Hök, “Critical review of non-invasive respiratory monitoring in medical care,” *Medical & Biological Engineering & Computing*, vol. 41, no. 4, pp. 377–383, Jul. 2003, doi: 10.1007/bf02348078.
- [14] A. Bonfiglio and D. De Rossi, “Wearable Monitoring Systems,” *Springer US eBooks*, Jan. 2011, doi: 10.1007/978-1-4419-7384-9.
- [15] I. Locher, M. Klemm, T. Kirstein, and G. Tröster, “Design and Characterization of Purely Textile Patch Antennas,” *IEEE Transactions on Advanced Packaging*, vol. 29, no. 4, pp. 777–788, Nov. 2006, doi: 10.1109/tadvp.2006.884780.
- [16] R. Salvado, C. Loss, R. F. Gonçalves, and P. Pinho, “Textile Materials for the Design of Wearable Antennas: A Survey,” *Sensors*, vol. 12, no. 11, pp. 15841–15857, Nov. 2012, doi: 10.3390/s121115841.
- [17] Z. Wang, L. Zhang, D. Psychoudakis, and J. L. Volakis, “Flexible textile antennas for body-worn communication,” *International Workshop on Antenna Technology*, Mar. 2012, doi: 10.1109/iwat.2012.6178647.
- [18] C. Hertleer, H. Rogier, L. Vallozzi, and L. Van Langenhove, “A Textile Antenna for Off-Body Communication Integrated Into Protective Clothing for Firefighters,” *IEEE Transactions on Antennas and Propagation*, vol. 57, no. 4, pp. 919–925, Apr. 2009, doi: 10.1109/tap.2009.2014574.
- [19] T. Kaija, J. Lilja, and P. Salonen, “Exposing textile antennas for harsh environment,” *Military Communications Conference*, Oct. 2010, doi: 10.1109/milcom.2010.5680300.
- [20] N. Liu, Y. Lu, S. Qiu, and P. Li, *Electromagnetic properties of electro-textiles for wearable antennas applications*, vol. 6, no. 4. Springer Science+Business Media, 2011, pp. 563–566. doi: 10.1007/s11460-011-0182-7.
- [21] S. Brebels *et al.*, “SOP Integration and Codesign of Antennas,” *IEEE Transactions on Advanced Packaging*, vol. 27, no. 2, pp. 341–351, Sep. 2004, doi: 10.1109/tadvp.2004.828822.
- [22] D. M. Pozar, *Microwave Engineering*. John Wiley & Sons, 2011.

- [23] J. M. H. Moll and V. Wright, "An objective clinical study of chest expansion.," *Annals of the Rheumatic Diseases*, vol. 31, no. 1, pp. 1–8, Jan. 1972, doi: 10.1136/ard.31.1.1.
- [24] C. Gabriel, "Compilation of the Dielectric Properties of Body Tissues at RF and Microwave Frequencies.," -, Jan. 1996, doi: 10.21236/ada303903.
- [25] X. Hui and E. C. Kan, "Monitoring vital signs over multiplexed radio by near-field coherent sensing," *Nature Electronics*, vol. 1, no. 1, pp. 74–78, Jan. 2018, doi: 10.1038/s41928-017-0001-0.
- [26] M. Wagih, A. S. Weddell, and S. Beeby, "Omnidirectional Dual-Polarized Low-Profile Textile Rectenna With Over 50% Efficiency for Sub- $\mu\text{W}/\text{cm}^2$ Wearable Power Harvesting," *IEEE Transactions on Antennas and Propagation*, vol. 69, no. 5, pp. 2522–2536, May 2021, doi: 10.1109/tap.2020.3030992.
- [27] A. S. Tajin, C. Amanatides, G. Dion, and K. R. Dandekar, "Passive UHF RFID-Based Knitted Wearable Compression Sensor," *IEEE Internet of Things Journal*, vol. 8, no. 17, pp. 13763–13773, Sep. 2021, doi: 10.1109/jiot.2021.3068198.
- [28] M. Roudjane, M. K. Khalil, A. Miled, and Y. Messaddeq, "New Generation Wearable Antenna Based on Multimaterial Fiber for Wireless Communication and Real-Time Breath Detection," *Photonics*, vol. 5, no. 4, p. 33, Oct. 2018, doi: 10.3390/photonics5040033.
- [29] M. Wagih, O. Malik, A. S. Weddell, and S. Beeby, "E-Textile Breathing Sensor Using Fully Textile Wearable Antennas," *E-Textiles 2021*, Mar. 2022, doi: 10.3390/engproc2022015009.
- [30] S. K. Noor, N. Ramli, N. M. Sahar, and T. Khalifa, "Compact and Wide Bandwidth Microstrip Patch Antenna for 5G Millimeter Wave Technology: Design and Analysis," *Journal of Physics*, vol. 1878, no. 1, p. 012008, May 2021, doi: 10.1088/1742-6596/1878/1/012008.
- [31] S. A. R. Parizi, "Bandwidth Enhancement Techniques," in *InTech eBooks*, 2017. doi: 10.5772/intechopen.70173.
- [32] R. Khatun, M. Rahman, and A. R. Md. T. Islam, "Design of a Compact Rectangular Microstrip Patch Antenna for 2.45 GHz ISM Band," *International Journal of Recent Engineering Science*, vol. 8, no. 3, pp. 30–35, Jun. 2021, doi: 10.14445/23497157/ijres-v8i3p105.
- [33] M. Yang, Z. Chen, P. S. Lau, X. Qing, and X. Yin, "Miniaturized Patch Antenna With Grounded Strips," *IEEE Transactions on Antennas and Propagation*, vol. 63, no. 2, pp. 843–848, Feb. 2015, doi: 10.1109/tap.2014.2382668.

- [34] H. Davoudabadifarahani and B. Ghalamkari, "High efficiency miniaturized microstrip patch antenna for wideband terahertz communications applications," *Optik*, vol. 194, p. 163118, Oct. 2019, doi: 10.1016/j.ijleo.2019.163118.
- [35] A. M. A. Sabaawi and C. C. Tsimenidis, *Circular truncated patch antennas for energy harvesting applications*. 2013. doi: 10.1109/lapc.2013.6711922.
- [36] S. Gorgutsa, M. Blais-Roberge, J. Viens, S. LaRoche, and Y. Messaddeq, "User-Interactive and Wireless-Communicating RF Textiles," *Advanced Materials and Technologies*, May 2016, doi: 10.1002/admt.201600032.
- [37] P. Guay, S. Gorgutsa, S. LaRoche, and Y. Messaddeq, "Wearable Contactless Respiration Sensor Based on Multi-Material Fibers Integrated into Textile," *Sensors*, vol. 17, no. 5, p. 1050, May 2017, doi: 10.3390/s17051050.
- [38] J. E. Sanderson *et al.*, "Impact of Changes in Respiratory Frequency and Posture on Power Spectral Analysis of Heart Rate and Systolic Blood Pressure Variability in Normal Subjects and Patients with Heart Failure," *Clinical Science*, vol. 91, no. 1, pp. 35–43, Jul. 1996, doi: 10.1042/cs0910035.
- [39] L. Yardley, M. A. Gresty, A. M. Bronstein, and J. Beyts, "Changes in heart rate and respiration rate in patients with vestibular dysfunction following head movements which provoke dizziness," *Biological Psychology*, vol. 49, no. 1–2, pp. 95–108, Sep. 1998, doi: 10.1016/s0301-0511(98)00029-5.
- [40] J. G. Betts *et al.*, *Anatomy and Physiology*, 2nd ed. Houston, TX: OpenStax College, 2013. [Online]. Available: <https://openstax.org/books/anatomy-and-physiology-2e/pages/22-introduction>. [Accessed: Sept. 1, 2023].
- [41] "Human respiratory system | Description, Parts, Function, & Facts," *Encyclopedia Britannica*, Sep. 19, 1998. <https://www.britannica.com/science/human-respiratory-system/The-mechanics-of-breathing>.
- [42] C. A. Balanis, *Antenna Theory: Analysis and Design*, 4th ed. Hoboken, NJ: John Wiley & Sons, 2012. [Online]. Available: <https://www.wiley.com/en-ca/Antenna+Theory%3A+Analysis+and+Design%2C+4th+Edition-p-9781119178996>. [Accessed: Jan. 1, 2023].
- [43] Z. Hasan, A. Zaman, and A. Ahmed, "Design and Fabrication of a Circular Microstrip Patch Antenna for GPS Application," vol. 8, pp. 54-57, Aug. 29, 2017.
- [44] T. Kingsuwannaphong and V. Sittakul, "Compact circularly polarized inset-fed circular microstrip antenna for 5 GHz band," *Computers & Electrical Engineering*, vol. 65, pp. 554–563, Jan. 2018, doi: 10.1016/j.compeleceng.2017.02.027.

Appendix

MATLAB CODE FOR DIFFERENT S11 PATTERNS

```
% Data extraction for no breathing
x1 = data(:, 1);
x2 = data(:, 4);
No_Breathing_1 = data(:, 5);
x3 = data(:, 7);
No_Breathing_2 = data(:, 8);
x4 = data(:, 10);

% Calculate the average values
average_values1 = (No_Breathing_1 + No_Breathing_2) / 2;

window_size = 60; % Adjust the window size as desired

% Apply moving average to the average values
smoothed_average_values1 = movmean(average_values1, window_size);
smoothed_average_values1(1:6) = average_values1(1:6);

% Find the minimum value and its index in the smoothed curve
[min_value, min_index] = min(smoothed_average_values1); % Corrected here

% Plot the curves with smoothed average values for No Breathing
subplot(2, 2, 1)
plot(x2, No_Breathing_1, x3, No_Breathing_2, x2, smoothed_average_values1,
'LineWidth', 2);
title('No Breathing');
legend('No Breathing 1', 'No Breathing 2', 'Smoothed Average');
hold on
% Add a marker for the minimum value for No Breathing
hold on
plot(x2(min_index), smoothed_average_values1(min_index), 'gs', 'MarkerSize',
8, 'LineWidth', 3); % Corrected here
% Display the minimum value
min_value_text = sprintf('Minimum value: %.2f', min_value);

% Place text at the bottom-left corner
x_pos = 0; % Extract x-axis lower bound
y_pos = -50; % Extract y-axis lower bound
text_str = sprintf('Min Value: %.2f at %.2f GHz', min_value, x2(min_index)/1e9);
text(x_pos, y_pos, text_str, 'VerticalAlignment', 'bottom', 'HorizontalAlignment', 'left');
%%%%%%%%%%%%%%%%%%%%%%%%%%%%%%%%%%%%%%%%%%%%%%%%%%%%%%%%

% Data extraction for normal breathing
```

```

x4 = data(:, 10);
Normal_Breathing_1 = data(:, 11);
x5 = data(:, 13);
Normal_Breathing_2 = data(:, 14);
x8 = data(:, 22);
Normal_Breathing_3 = data(:, 23);

% Calculate the average values
average_values2 = (Normal_Breathing_1 + Normal_Breathing_2 +
Normal_Breathing_3) / 3;

% Apply moving average to the average values
smoothed_average_values2 = movmean(average_values2, window_size);
smoothed_average_values2(1:6) = average_values2(1:6);

% Find the minimum value and its index
[min_value, min_index] = min(smoothed_average_values2); % Corrected here

% Plot the curves for Normal Breathing
subplot(2, 2, 2)
plot(x4, Normal_Breathing_1, x5, Normal_Breathing_2, x8, Normal_Breathing_3, x4,
smoothed_average_values2, 'LineWidth', 2);
title('Normal Breathing');
legend('Normal Breathing 1', 'Normal Breathing 2', 'Normal Breathing 3', 'Smoothed
Average');

% Add a marker for the minimum value for Normal Breathing
hold on
plot(x4(min_index), smoothed_average_values2(min_index), 'gs', 'MarkerSize',
8, 'LineWidth', 3); % Corrected here
hold off

% Display the minimum value
min_value_text = sprintf('Minimum value: %.2f', min_value);

x_pos = 0;
y_pos = -30;
text_str = sprintf('Min Value: %.2f at %.2f GHz', min_value, x4(min_index)/1e9);
text(x_pos, y_pos, text_str, 'VerticalAlignment', 'bottom', 'HorizontalAlignment', 'left');
%%%%%%%%%%%%%%%%%%%%%%%%%%%%%%%%%%%%%%%%%%%%%%%%%%%%%%%%

% Data extraction for Slow breathing
x4 = data(:, 25);
Slow_Breathing_1 = data(:, 26);
x5 = data(:, 28);
Slow_Breathing_2 = data(:, 29);
x7 = data(:, 34);

```

```

Slow_Breathing_3 = data(:, 35);

% Calculate the average values
average_values3 = (Slow_Breathing_1 + Slow_Breathing_2 + Slow_Breathing_3) / 3;

% Apply moving average to the average values
smoothed_average_values3 = movmean(average_values3, window_size);
smoothed_average_values3(1:6) = average_values3(1:6);

% Find the minimum value and its index
[min_value, min_index] = min(smoothed_average_values3); % Corrected here

% Plot the curves for Slow Breathing
subplot(2, 2, 3)
plot(x4, Slow_Breathing_1, x5, Slow_Breathing_2, x7, Slow_Breathing_3, x4,
smoothed_average_values3, 'LineWidth', 2);
title('Slow Breathing');
legend('Slow Breathing 1', 'Slow Breathing 2', 'Slow Breathing 3', 'Smoothed Average');

% Add a marker for the minimum value for Slow Breathing
hold on
plot(x4(min_index), smoothed_average_values3(min_index), 'gs', 'MarkerSize',
8, 'LineWidth', 3); % Corrected here
hold off

% Display the minimum value
min_value_text = sprintf('Minimum value: %.2f', min_value);
x_pos = 0;
y_pos = -25;
text_str = sprintf('Min Value: %.2f at %.2f GHz', min_value, x4(min_index)/1e9);
text(x_pos, y_pos, text_str, 'VerticalAlignment', 'bottom', 'HorizontalAlignment', 'left');
%%%%%%%%%%%%%%

% Data extraction for Fast breathing
x5 = data(:, 43);
Fast_Breathing_1 = data(:, 44);
x7 = data(:, 49);
Fast_Breathing_2 = data(:, 50);
x8 = data(:, 52);
Fast_Breathing_3 = data(:, 53);

% Calculate the average values
average_values4 = (Fast_Breathing_1 + Fast_Breathing_2 + Fast_Breathing_3) / 3;

% Apply moving average to the average values
smoothed_average_values4 = movmean(average_values4, window_size);

```



```

smoothed_average_values4(1:6) = average_values4(1:6);

% Find the minimum value and its index
[min_value, min_index] = min(smoothed_average_values4); % Corrected here

% Plot the curves for Fast Breathing
subplot(2, 2, 4)
plot(x5, Fast_Breathing_1, x7, Fast_Breathing_2, x8, Fast_Breathing_3, x5,
smoothed_average_values4, 'LineWidth', 2);
title('Fast Breathing');
legend('Fast Breathing 1', 'Fast Breathing 2', 'Fast Breathing 3', 'Smoothed Average');

% Add a marker for the minimum value for Fast Breathing
hold on
plot(x5(min_index), smoothed_average_values4(min_index), 'gs', 'MarkerSize',
8, 'LineWidth', 3); % Corrected here
hold off

% Display the minimum value
min_value_text = sprintf('Minimum value: %.2f', min_value);

x_pos = 0;
y_pos = -30;
text_str = sprintf('Min Value: %.2f at %.2f GHz', min_value, x5(min_index)/1e9);
text(x_pos, y_pos, text_str, 'VerticalAlignment', 'bottom', 'HorizontalAlignment', 'left');
%%%%%%%%%%%%%%%%%%%%%%%%%%%%%%%%%%%%%%%%%%%%%%%%%%%%%%%%

% Plotting the comparison of average values
figure
p1 = plot(x1, smoothed_average_values1, '-r', 'LineWidth', 1.5); % Red line for No
Breathing average
hold on
p2 = plot(x1, smoothed_average_values2, '-g', 'LineWidth', 1.5); % Green line for
Normal Breathing average
p3 = plot(x1, smoothed_average_values3, '-b', 'LineWidth', 1.5); % Blue line for Slow
Breathing average
p4 = plot(x1, smoothed_average_values4, '-m', 'LineWidth', 1.5); % Magenta line for
Fast Breathing average

% Annotate each curve with its respective minimum frequency and draw vertical bold
dotted lines

% No Breathing
[min_val_1, min_index_1] = min(smoothed_average_values1);
plot([x1(min_index_1), x1(min_index_1)], [min(average_values1),
max(average_values1)], '--r', 'LineWidth', 2);

```

```

text(x1(1), average_values1(min_index_1), sprintf('No Breathing: %.2f GHz',
x1(min_index_1)/1e9), 'Color', 'r', 'VerticalAlignment', 'bottom');

% Normal Breathing
[min_val_2, min_index_2] = min(smoothed_average_values2);
plot([x1(min_index_2), x1(min_index_2)], [min(average_values2),
max(average_values2)], '--g', 'LineWidth', 2);
text(x1(1), average_values2(min_index_2), sprintf('Normal Breathing: %.2f GHz',
x1(min_index_2)/1e9), 'Color', 'g', 'VerticalAlignment', 'bottom');

% Slow Breathing
[min_val_3, min_index_3] = min(smoothed_average_values3);
plot([x1(min_index_3), x1(min_index_3)], [min(average_values3),
max(average_values3)], '--b', 'LineWidth', 2);
text(x1(1), average_values3(min_index_3), sprintf('Slow Breathing: %.2f GHz',
x1(min_index_3)/1e9), 'Color', 'b', 'VerticalAlignment', 'bottom');

% Fast Breathing
[min_val_4, min_index_4] = min(smoothed_average_values4);
plot([x1(min_index_4), x1(min_index_4)], [min(average_values4),
max(average_values4)], '--m', 'LineWidth', 2);
text(x1(1), average_values4(min_index_4), sprintf('Fast Breathing: %.2f GHz',
x1(min_index_4)/1e9), 'Color', 'm', 'VerticalAlignment', 'bottom');

% Title and Legend
title('Comparison Between Different Breathing Patterns and No Breathing');
legend('No Breathing', 'Normal Breathing', 'Slow Breathing', 'Fast Breathing');

hold off

%%%%%%%%%%%%%%

% Simulation vs Practical comparison
a = data1(:,1)*10e8;
b = data1(:,2);
[min_value_CST, min_index_CST] = min(b);
[min_value_practical, min_index_practical] = min(smoothed_average_values1);

smoothed_average_values1(1:6,1) = average_values1(1:6,1);
figure
plot(a, b, 'b-', x1, smoothed_average_values1, 'r-')
title('Simulation vs Practical');
xlim([2e9, 3e9]); % Limit the x-axis to 2-3 GHz
legend('Practical No Breathing', 'Simulated No Breathing');

% Adding a horizontal line at -10 dB
hold on;

```

```

yline(-10, 'k--', 'LineWidth', 1.5);

% Finding intersection points for practical values
diff_values_practical = smoothed_average_values1 + 10;
zero_crossings_practical = find(diff(diff_values_practical >= 0));
x_intersect_practical = x1(zero_crossings_practical);

% Finding intersection points for CST values
diff_values_CST = b + 10;
zero_crossings_CST = find(diff(diff_values_CST >= 0));
x_intersect_CST = a(zero_crossings_CST);

% Check intersection point lengths
if length(x_intersect_practical) >= 2
    f_low_practical = x_intersect_practical(1);
    f_high_practical = x_intersect_practical(2);
    BW_practical = (f_high_practical - f_low_practical) / sqrt(f_high_practical *
f_low_practical);
    BW_text_practical = sprintf('BW (Practical): %.2f GHz', (BW_practical)*100);
    text(0.05, 0.9, BW_text_practical, 'Color', 'r', 'Units', 'normalized');
end

if length(x_intersect_CST) >= 2
    f_low_CST = x_intersect_CST(1);
    f_high_CST = x_intersect_CST(2);
    BW_CST = (f_high_CST - f_low_CST) / sqrt(f_high_CST * f_low_CST);
    BW_text_CST = sprintf('BW (CST): %.2f GHz', BW_CST);
    text(0.05, 0.85, BW_text_CST, 'Color', 'b', 'Units', 'normalized');
end

% Plotting and annotating intersection points
plot(x_intersect_practical, repmat(-10, size(x_intersect_practical)), 'ro', 'MarkerSize', 6,
'LineWidth', 1.5);
plot(x_intersect_CST, repmat(-10, size(x_intersect_CST)), 'bo', 'MarkerSize', 6,
'LineWidth', 1.5);

for i = 1:length(x_intersect_practical)
    annotation_str = sprintf('Practical Intersection: %.2f GHz',
x_intersect_practical(i)/1e9);
    text(x_intersect_practical(i), -11 - (i-1)*2, annotation_str, 'Color', 'r',
'HorizontalAlignment', 'center');
end

for i = 1:length(x_intersect_CST)
    annotation_str = sprintf('CST Intersection: %.2f GHz', x_intersect_CST(i)/1e9);
    text(x_intersect_CST(i), -13 - (i-1)*2, annotation_str, 'Color', 'b',
'HorizontalAlignment', 'center');
end

```

```

end

% Calculating bandwidths for each set of intersections
if length(x_intersect_practical) >= 2
    BW_practical = (x_intersect_practical(2) - x_intersect_practical(1)) /
sqrt(x_intersect_practical(2) * x_intersect_practical(1));
    BW_text_practical = sprintf('BW (Practical): %.5f %!', BW_practical*100); %
increased precision to 5 decimal places
    text(0.05, 0.05, BW_text_practical, 'Color', 'r', 'Units', 'normalized');

    % Print the result to MATLAB console for clarity
    disp(['Practical Bandwidth: ', num2str(BW_practical), ' %']);
end

if length(x_intersect_CST) >= 2
    BW_CST = (x_intersect_CST(2) - x_intersect_CST(1)) / sqrt(x_intersect_CST(2) *
x_intersect_CST(1));
    BW_text_CST = sprintf('BW (CST): %.5f %Percent', BW_CST*100); % increased
precision to 5 decimal places
    text(0.05, 0.15, BW_text_CST, 'Color', 'b', 'Units', 'normalized');

    % Print the result to MATLAB console for clarity
    disp(['CST Bandwidth: ', num2str(BW_CST), ' %']);
end

% Display resonance frequency for both curves
resonance_freq_CST = a(min_index_CST);
resonance_freq_practical = x1(min_index_practical);

% Plotting and annotating the resonance frequencies
plot(resonance_freq_CST, min_value_CST, 'bx', 'MarkerSize', 6, 'LineWidth', 1.5);
plot(resonance_freq_practical, min_value_practical, 'rx', 'MarkerSize', 6, 'LineWidth',
1.5);

resonance_annotation_CST = sprintf('Resonance (CST): %.2f GHz, %.2f dB',
resonance_freq_CST/1e9, min_value_CST);
resonance_annotation_practical = sprintf('Resonance (Practical): %.2f GHz, %.2f dB',
resonance_freq_practical/1e9, min_value_practical);

% Displaying the annotations on the right side
text(0.95, 0.2, resonance_annotation_CST, 'Color', 'b', 'Units', 'normalized',
'HorizontalAlignment', 'right');
text(0.95, 0.15, resonance_annotation_practical, 'Color', 'r', 'Units', 'normalized',
'HorizontalAlignment', 'right');
% Legend
legend('CST Values', 'Practical', '-10 dB', 'Practical Intersections', 'CST Intersections');

```

MATLAB CODE FOR BREATHING RATE ESTIMATION

```
% Sort the data by frequencies
CST = sortrows(trial, 1);

% Remove duplicate frequencies
[frequencies, unique_indices] = unique(CST(:, 1), 'stable');
s11_magnitudes = CST(unique_indices, 2);
s11_phases = CST(unique_indices, 3);

% Smooth the data
smooth_window = 5; % Window width for moving average smoothing
smoothed_magnitudes = smooth(s11_magnitudes, smooth_window);
smoothed_phases = smooth(s11_phases, smooth_window);

% Find the resonance frequency index
[~, resonance_freq_idx] = min(smoothed_magnitudes);

% Split the phase data into before and after resonance
before_resonance_phase = smoothed_phases(1:resonance_freq_idx);

% Create the mirrored phase
adjusted_phase = [before_resonance_phase; -flip(before_resonance_phase)];

% Adjust the phase length
if length(adjusted_phase) > length(frequencies)
    adjusted_phase = adjusted_phase(1:length(frequencies));
elseif length(adjusted_phase) < length(frequencies)
    padding = ones(length(frequencies) - length(adjusted_phase), 1) *
adjusted_phase(end);
    adjusted_phase = [adjusted_phase; padding];
end

% Other calculations
s11_linear = 10.^(smoothed_magnitudes./20);
s11_complex = s11_linear .* exp(1i * deg2rad(adjusted_phase));
s11_time = ifft(s11_complex);
RSSI_dBm = -10 * log10(abs(s11_time));

N = length(RSSI_dBm);

time = linspace(0, (N-1)*dt, N);

% Identify peaks and troughs from the RSSI data
[~, initial_peak_locs] = findpeaks(RSSI_dBm, 'MinPeakProminence', 0.5,
'MinPeakDistance', 5);
```

```

[~, initial_trough_locs] = findpeaks(-RSSI_dBm, 'MinPeakProminence', 0.5,
'MinPeakDistance', 10);

% Combine initial detected peaks and troughs for the purpose of interpolation
all_points = [initial_peak_locs; initial_trough_locs];
all_values = [RSSI_dBm(initial_peak_locs); RSSI_dBm(initial_trough_locs)];

% Sort all points in increasing order
[all_points, sortIdx] = sort(all_points);
all_values = all_values(sortIdx);

% Create an interpolated signal based on peaks and troughs
breathing_pattern = interp1(all_points, all_values, 1:N, 'pchip', 'extrap');

% Identify peaks and troughs from the estimated breathing pattern
[~, peak_locs] = findpeaks(breathing_pattern, 'MinPeakProminence', 0.5,
'MinPeakDistance', 5);
[~, trough_locs] = findpeaks(-breathing_pattern, 'MinPeakProminence', 0.5,
'MinPeakDistance', 5);

% Trim the RSSI curve so it starts and ends at a trough
if ~isempty(trough_locs)
    first_trough = trough_locs(1);
    last_trough = trough_locs(end);

    % Trim the data arrays
    time = time(first_trough:last_trough);
    RSSI_dBm = RSSI_dBm(first_trough:last_trough);
    breathing_pattern = breathing_pattern(first_trough:last_trough);
    s11_time = s11_time(first_trough:last_trough); % Add this line to trim s11_time as
well.

    % Update the peak and trough locations after trimming
    peak_locs = peak_locs - first_trough + 1;
    trough_locs = trough_locs - first_trough + 1;
end

% Detect breathing cycles: two troughs and the largest peak in between
breathing_cycles = [];

for i = 1:length(trough_locs)-1
    current_trough = trough_locs(i);
    next_trough = trough_locs(i+1);

    % Extract peaks between current_trough and next_trough
    middle_peaks = peak_locs(peak_locs > current_trough & peak_locs < next_trough);

```

```

if ~isempty(middle_peaks)
    peak_amplitudes = breathing_pattern(middle_peaks);

    % If any peak exceeds 35 in amplitude, consider it as the max
    large_peak_idx = find(peak_amplitudes > 35);
    if ~isempty(large_peak_idx)
        main_peak = middle_peaks(large_peak_idx(1));
    else
        [~, max_idx] = max(peak_amplitudes);
        main_peak = middle_peaks(max_idx);
    end

    breathing_cycles = [breathing_cycles; [current_trough, main_peak, next_trough]];
end
end

if isempty(breathing_cycles)
    fprintf('No breathing cycles detected based on the criteria.\n');
else
    % Calculate breathing durations
    breathing_durations = time(breathing_cycles(:,3)) - time(breathing_cycles(:,1));
    avg_breathing_duration = mean(breathing_durations);

    fprintf('The average breathing cycle duration is %.2f seconds.\n',
    avg_breathing_duration);
end

if isempty(breathing_cycles)
    fprintf('No breathing cycles detected based on the criteria.\n');
else
    % Calculate breathing durations
    breathing_durations = time(breathing_cycles(:,3)) - time(breathing_cycles(:,1));
    avg_breathing_duration = mean(breathing_durations);
    fprintf('The average breathing cycle duration is %.2f seconds.\n',
    avg_breathing_duration);

    % Estimate breathing rate from the average duration
    breathing_rate = 60 / avg_breathing_duration * 1e-8; % in breaths per minute
    fprintf('Estimated breathing rate is %.2f breaths per minute.\n', breathing_rate);
end

% Plotting
figure;
subplot(2,1,1); % Two subplots for S11 magnitude and phase
plot(frequencies, smoothed_magnitudes, 'b', 'LineWidth', 1.5);
xlabel('Frequency (Hz)');

```

```

ylabel('Magnitude (dB)');
title('Updated S11 Magnitude');
grid on;

subplot(2,1,2);
plot(frequencies, smoothed_phases, 'r', 'LineWidth', 1.5);
xlabel('Frequency (Hz)');
ylabel('Phase (degrees)');
title('Updated S11 Phase');
grid on;

% Plotting the magnitude of the DIFT complex values
figure;
plot(time, abs(s11_time), 'k-', 'LineWidth', 1.5);
xlabel('Time (s)');
ylabel('Magnitude');
title('Magnitude of Inverse Fast Fourier Transform of S11');
grid on;

figure;
plot(time, RSSI_dBm, 'k-', 'LineWidth', 1.5); % original DIFT data
xlabel('Time (s)');
ylabel('IFFT (dBm)');

title('dBm of IFFT of S11');
grid on;
hold on;

plot(time, breathing_pattern, 'b-', 'LineWidth', 2); % estimated breathing pattern

for cycle = 1:size(breathing_cycles, 1)
    plot(time(breathing_cycles(cycle, 2)), breathing_pattern(breathing_cycles(cycle, 2)),
    'ro', 'MarkerSize', 10, 'LineWidth', 1.5); % Peaks used in breathing cycle estimation
    plot(time(breathing_cycles(cycle, [1, 3])), breathing_pattern(breathing_cycles(cycle, [1,
    3])), 'gs', 'MarkerSize', 10, 'LineWidth', 1.5); % Troughs used in breathing cycle
    estimation
end

legend('Original IFFT dBm', 'Estimated Breathing Pattern', 'Used Peaks', 'Used
Troughs');

hold off;

```


The logo of the United Arab Emirates University (UAEU) is displayed in a red rectangular box. It consists of the letters 'UAEU' in a white, bold, sans-serif font.

جامعة الإمارات العربية المتحدة
United Arab Emirates University



UAE UNIVERSITY MASTER THESIS NO. 2023: 77

The antenna, fabricated from a thin copper adhesive sheet, demonstrates compatibility with textile materials of low thickness and a relative permittivity of 1.3. Using CST Studio Suite 3D EM simulation software, the antenna's design was optimized through extensive trials, achieving improved bandwidth and gain. Our findings indicate that the antenna successfully differentiates between various breathing patterns, including slow, normal, and fast breathing rates.

Mo'ath AL Hayek received his Master of Science in Electrical Engineering from the Department of Electrical & Communication Engineering, College of Engineering at UAE University, UAE. He received his Bachelor of Science in Electrical Engineering from the College of Engineering, Al Balqa' Applied University, Jordan.

www.uaeu.ac.ae

Online publication of thesis:
<https://scholarworks.uaeu.ac.ae/etds/>

UAEU عمادة المكتبات
Libraries Deanship

جامعة الإمارات العربية المتحدة
United Arab Emirates University



قسم الخدمات المكتبية الرقمية - Digital Library Services Section